JAERI-M
6605

10-CHANNEL NEUTRAL PARTICLE ENERGY ANALYSER APPARATUS AND ITS APPLICATION TO TOKAMAK PLASMAS

July 1976

H. TAKEUCH, A. FUNAHASHI, K. TAKAHASHI,
H. SHIRAKATA and S. YANO*

日本原子力研究所
Japan Atomic Energy Research Institute

JAERI - M 6605

10-Channel Neutral Particle Energy Analyser Apparatus and its Application to Tokamak Plasmas

Hiroshi TAKEUCHI, Akimasa FUNAHASHI, Koki TAKAHASHI,
Hirofumi SHIRAKATA and Syukuro YANO*
Division of Thermonuclear Fusion Research, Tokai, JAERI

(Received June 7, 1976)

A 10-channel neutral particle energy analyser apparatus for measurement of charge-exchange fast atoms emitted from a hot tokamak plasma has been constructed to determine the ion temperature of plasma from fewer discharge shots and to improve the accuracy of measurement. It consists of a 45-degrees parallel plate electrostatic analyser with ten ion detectors (Ceratron multipliers), a charge stripping cell, a dry vacuum pumping system and pulse-counting circuits for data acquisition. A calibration experiment of the apparatus is made for the particle energy and the energy resolution with electron beams of 100 to 1000 eV. The transmission efficiency of particles in the energy analyser is measured with proton beams of 1, 2 and 3 keV, and the conversion efficiency for H_2 gas in a charge stripping cell is also determined with hydrogen-atom beams of 2, 3 and 4 keV. It is confirmed from the calibration experiments that the 10-channel neutral particle energy analyser apparatus has the characteristics expected from its design and can operate to determine ion temperatures for JAERI-tokamak devices.

Ion temperatures of JFT-2a and JFT-2 devices were measured with this apparatus, in order to check the usefulness and reliability of the apparatus and to investigate the parameter dependence of ion temperatures. It is found that an ion temperature can be measured with sufficient accuracy from six plasma shots (three shots to determine particle signals and three shots to determine background noises). The peak ion temperatures 80 to 400 eV

---

* Kobe Mercantile Marine College

are about (1/2 - 1/3) of the central electron temperatures. Dependence of the ion temperatures on plasma current I_p, toroidal magnetic field B_t and average electron density $\bar{n}_e$ is investigated for I_p = 15 to 170 kAmp, B_t = 10 to 18 kGauss and $\bar{n}_e = (0.8 \text{ to } 1.8) \times 10^{13}$ cm^{-3} on JFT-2a and JFT-2 devices. It is shown that the ion temperatures are in good agreement with the scaling law by Artsimovich $T_i \propto (I_p B_t \bar{n}_e R^2)^{1/3}$, with R as the major radius of a tokamak device.

10チャンネル中性粒子エネルギー分析装置とそのトカマクプラズマへの適用

日本原子力研究所，東海研究所
核融合研究部

竹内　浩・船橋昭昌・高橋興起
白形弘文・矢野淑郎*

（1976年6月7日受理）

イオン温度測定のためのプラズマショット数の減少と測定精度の向上のために，トカマクプラズマ用の10チャンネル中性粒子エネルギー分布装置を製作した。この装置は45度入射型平行板静電エネルギー分析器，10個のイオン検出器（セントロン増幅器），電荷ストリッピングセル，オイルフリーな真空排気系，パルス計数データ収集システムからなっている。またエネルギー分析器の較正は100 eVから1000 eVの電子ビームを用いて，粒子エネルギーと偏向板電圧の関係，エネルギー分解能について行なわれた。分析器における透過効率は1, 2および3 keVのプロトンビームを用いて決定され，また電荷交換セルにおける，H_2 ガスの交換効率は2, 3および4 keVの水素原子ビームを用いて測定された。これらの較正実験より10チャンネル中性粒子エネルギー分析装置は設計値から予想された特性を持っており，また原研のトカマク装置におけるイオン温度を決定するために作動出来得ることが確認された。

10チャンネル中性粒子エネルギー分析装置の有用性と信頼性を確かめるためと，JFT－2a，JFT－2トカマクにおけるイオン温度のパラメーター依存性を調べるために，JFT－2a，JFT－2のイオン温度測定がこの分析装置を用いて行なわれた。これらの測定において，イオン温度は6ショット（粒子信号を測定するために3ショット，バックグラウンド雑音を決定するために3ショット）で充分な信頼性を持って，決定できることがわかった。測定されたピーク温度80 eV～400 eVは中心の電子温度の約（1／2～1／3）であった。JFT－2a，JFT－2におけるイオン温度のプラズマ電流I_p，トロイダル磁場B_t，平均電子密度n_eの依存性がI_p＝15～170 kA，B_t＝10～18 kG，n_e＝0.8～1.8×10^{13} cm^{-3} に対して調べられた。そのイオン温度はArtsimouich のスケーリング則$T_i \propto (I_p B_t n_e R^2)^{1/3}$と良く一致することがわかった。

＊　神戸商船大学　原子力動力科

CONTENTS

1. INTRODUCTION

The determination of ion temperatures in magnetically confined plasmas has often been studied on energy analysis of charge-exchanged, fast neutral particles. The temperature is determined by measurements of the energy distribution of the fast neutral particles which can escape freely from the confinement magnetic field. Therefore the measurement by this method in principle is not influenced by the confinement magnetic field. The fast neutral particles are produced through resonance charge exchange collisions of ions (protons) with cold neutral atoms (hydrogen atoms), i.e., H^+ (hot) + H^0 (cold) $\longrightarrow$ H^0 (fast) + H^+ (cold). In the process the energy of the hot ions is transfered to the secondary, fast atoms without significant energy loss. Thus the energy distribution of fast neutral atoms reflects that of ions in a hot plasma region with sufficient accuracy, if the distortion effects due to re-trapping can be neglected, by ionization and inverse charge-exchange processes.

In most cases the energy analysis of fast neutral particles are ionized through collisions with neutral gases in a charge stripping cell and the energies of ionized particles are analysed with an electrostatic energy analyser. The first success of this method was shown by Afrosimov et al. in 1961.[1] Since then several papaers[2-5] have been published on the determination of the ion temperature by this method. Recently the analysis of the charge-exchanged particles has become a standard method of measurement of hot ion temperatures. Several methods of energy analysis and ion detection have been used. For example, Afrosimov et al.[1] used a condenser-type electrostatic analyser and a Daly-type ion detector (consisting of a secondary electron emission knob, a scintillator and a photomultiplier). Noda et al.[5] and Fleischmann and Tuckfield[6] adopted 127°17' and 126 cylindrical electro-static energy analysers respectively and a Daly-type ion detector. Barnett and Ray[7] made use of a 45° parallel plate electrostatic energy analyser and a channel-type secondary electron multiplier as the ion detector. In these works, fast neutral particles which are ionized in a charge stripping cell are energy-analysed. Ferguson and Kidd[8], in their energy analysis of neutral particles emitting from θ-pinched plasmas, used a rotating disk and measured the energy of particles from a time of flight for the particles instead of using a stripping cell and ion detector. In their analysis an electron emission was used for the detection of neutral particles.

Expect the method used by Ferguson and Kidd, the above-mentioned

analyser systems can measure only a single point on the particle energy distribution per a discharge of pulsed plasma devices (in fact, several discharges are often necessary to obtain the single point in order to confirm the reproducibility of plasmas and to examine the level of background noises). Therefore many discharges are needed to determine the energy distribution. Such circumstances produce uncertainty in the ion temperature determination and inevitably require much time and effort of investigators. In order to solve the difficulties of a single-channel analyser two improvements were proposed and have been performed mainly for diagnoses of tokamak plasmas. One is an application of sawtooth electric field to be electrodes of a cylindrical electrostatic energy analyser (TFR[10a]) and Alcator[10b] tokamaks). Another is to use a multi-channel electrostatic analyser (T-4[11a]) ORMAK[11b]) and Princeton[11c]) tokamaks) which is capable of measuring several points on the energy distribution during a single discharge.

Since the formar method is applicable to a single channel analyser, the device is rather compact in size and fabricated economically. However, emitted neutral particles with different energies are detected at different time points. Therefore in order to determine ion temperatures, it is implicity assumed that a plasma does not change significantly during the period of a scanning time of the sawtooth electric field. On the other hand in a multi-channel system the ion temperatures can be determined without such an assumption. It seems that the extention to the multi-channel analyser is preferential for research of tokamak plasmas, because of capability of continuous measurements. Ferguson and Kidd's method can measure many points on the particle energy distribution.[8] A drift tube to measure the time of flight is rather long (for example, 6.6 m for a plasma of 100 eV). As an apparatus becomes very large for measurements of temperatures higher than a few hundred eV, their method has not been used for diagnoses of high-temperature tokamak plasmas.

In our institute a 10-ch neutral particle energy analyser for JAERI-tokamak devices has been designed employing the data obtained from the measurements of JFT-2 tokamak plasma with a single-channel analyser[12] and calibration experiments in the analyser[13]. The neutral particle energy analyser apparatus (here after, abbreviated to 10-ch NPEAA or NPEAA) are equipped with ten channel-type multipliers to detect resulting ions converted from charge-exchanged, fast particles in a gas cell. The energy difference between ch-1 and ch-10 is of an order, and energy resolution is

50 % (ch-1) to 7.6 % (ch-10).

In Section 2 we describe each part of 10-ch NPEAA, i.e., an electrostatic analyser, ion detectors, a data acquisition system, and a vacuum pumping system. Section 3 provides results on calibration experiments of the particle energy and transmission coefficient in the analyser and stripping cell efficiency. In Section 4 we show the experimental arrangements for neutral particle measurements in JAERI devices (JFT-2a, noncircular cross-section tokamak with a divertor and JFT-2, fat tokamak). This section describes the results on ion temperature measurement in these devices, and noise sources encountered in the measurements. From these measurements it is confirmed that ion temperatures of JFT-2a or JFT-2 plasmas can be determined in several discharges with the 10-ch NPEAA. In Section 5 the measured temperatures are shown against various plasma parameters and compared with the scaling law by Artsimovich. Section 6 discusses the results. Finally, in section 7 we summarize the results.

2. DESCRIPTION OF 10-CHANNEL NEUTRAL PARTICLE ENERGY ANALYSER APPARATUS

The schematic diagram of 10-ch NPEAA is shown in Fig. 1. Charge-exchanged fast, neutral particles leaking from plasmas are ionized by collisions with H_2 moleculars which are reserved in a charge stripping cell. The H_2 gas is fed into the charge stripping cell through a needle valve at a constant flow velocity. The pressure in the stripping cell is held at about a few 10^{-4} torr by a differential pumping. The differential pumping generates a two-order pressure difference between the charge stripping cell and other parts of the analyser with a sputter ion pump whose pumping speed is 1000 ℓ/sec. The vacuum pumping system for the NPEAA and a drift tube connected to a plasma device consists of oil-free, dry vacuum pumps, in order to minimize contaminations of ion detectors due to oil-vapors and unfavorable effects to measured plasmas or the plasma device. The vacuum pump for the drift tube will be described in Section 4.

The resulting ions produced in the charge stripping cell enter the energy analyser. The energy analyser is a 45-degrees parallel plate electro-static analyser equipped with ten ion detectors. It is designed to be an extention of a Harrower-type analyser[14] to a multi-channel one. A line drawing of the 10-ch electro-static analyser is shown in Fig. 2. The ions from the charge stripping cell enter an electro-static field produced by a deflecting plate which is set at 45 degrees to the incident beam. The ions drifting into the field have different parabolic orbits according to their energies. Consequently the ions arrive at specified positions in the output channel of the analyser corresponding to their energies. The relation between the incident ion energy E and the voltage applied to the deflecting plate V, the energy resolution of total signal width dV/V, the displacement B at the output channel due to the shift of the incident angle, and the displacement dX at the output channel due to the shift of the incident point are given as follows respectively;[14]

$$V = \frac{2d}{X} E \tag{1}$$

$$\frac{dV}{V} = \frac{dX_1+dX_2}{2X} (1+\sec 2\Delta\theta) - (1-\sec 2\Delta\theta) \tag{2}$$

$$B = 2X \cdot |\Delta\theta| \tag{3}$$

$$dX = dX' \tag{4}$$

where d is a distance between the deflecting and the earth plates, X a distance from the center of the incident slit to that of the exit slit, dX_1 a width of the incident slit, dX_2 a width of the exit slit, dX' a distance between the incident point and the center of the indicent slit, and $\Delta\theta$ angle of shift from the normal incident angle (45 degrees). In addition, expressions of d and dX_2, and the height of the exit slit h are given by Eq. (5) and (6);

$$d > d_{min} \equiv \frac{X}{4}(1+2\cdot\Delta\theta) \tag{5}$$

$$dX_2 > B + dX_1 \tag{6a}$$

$$h > 2X\cdot|\Delta\theta| \tag{6b}$$

If the value of $\Delta\theta$ is small, Equation (2) becomes Eq. (7);

$$\frac{dV}{V} = \frac{dX_1 - dX_2}{X} \tag{7}$$

The designed values of X, 2d/X, dX_2, dV/V, and h in each channel of the 10-ch NPEAA are shown in Table 1. The value of d is chosen to be $d \cong 1.5 \times d_{min}$, i.e., d = 90 mm. The incident slit is selected to be circular aperture with its diameter of 5.92 mm so that sufficient neutral particles can enter the analyser for determing ion temperatures in JFT-2 and JFT-2a devices. In addition, to obtain the maximum level of particle signals, it is desirable that all particles entering the analyser come to the output channel without any particle losses. Thus the aperture sizes of the exit slit (width dX_2, and height h, as shown in Table 1) are determined from Eqs. (5), (6a) and (6b) for dX_1 = 5.92 mm and the maximum value of $\Delta\theta$ ($\Delta\theta_{max} \cong 0.44$ deg). The value of $\Delta\theta_{max}$ is determined from the aperture sizes of incident slits of the charge stripping cell (4 mm inner diameter) and the analyser, and the distance between these slits (about 26 cm). The channel number of the analyser is chosen to be ten, and the energy difference is an one-order between ch-1 corresponding to the lowest energy and ch-10 to the highest energy.

The deflecting plate and earth plate of the NPEAA are made of stainless steel (SUS 304). To reduce the distortion of electric field, four guard-plate electrodes are installed between the deflecting and earth plate. There is a hole in the deflecting plate, so as to let out photons emitted

from a plasma and neutral particles which are not ionized in the charge stripping cell. Also we installed shadow masks (stainless steel meshes) in front of the exit slits to reduce the field distortion coming from high voltage (-4.5 kV) applied to channel-type secondary electron multipliers, Ceratrons which are used as ion detectors of the energy analyser. These Ceratons (EMW-1081B type) are fixed behind the exit apertures of the earth plate, as shown in Fig. 2.

The Ceratron multiplier is made of Ceramics. Each Ceratron operates in the pulse saturation mode. The operating method of Ceratron is illustrated in Fig. 3. The gain of EMW-1081B Ceratron is about 10^8 and the width of output pulse is about 2 nanosecond. The high voltages to operate each Ceratron are supplied by one power supply. The Ceratrons being placed inside the analyser which is evacuated with a sputter ion vacuum pump, ions resulting in the sputter ion pump might enter them. Hence the Ceratrons are placed in positions distant from a pumping port of the NPEAA. We also installed a screen at the pumping port to prevent ions in the pump from entering a vacuum chamber of the analyser. Each Ceratron is separated by a shield of stainless steel in the Ceratron box to reduce mutual electrical interactions among them. All lead wires in the vacuum chamber are electrically shielded between Ceratrons and output connectors. As a result of above-mentioned device electrical noises of Ceratrons can be decreased down to 2 --- 50 counts/minute.

Ceratrons being operated in the saturation mode, we adopt a data acquisition system of pulse-counting method. The block diagram of pulse-counting, electric circuits is shown in Fig. 4. The signal from Ceratron in each channel pass through differential circuits, preamplifiers and linear amplifiers. And the signals are separated from thermal noise levels with discriminators and are counted with ten scalers. The count numbers from the scalers are transferred into memory cores through a multiplxer. The characteristics of sampling scalers for 10-ch neutral analysis are shown in Table 2. The sampling number is ten per channel. Therefore the total number of the memory cores is 100. The sampling time can be chosen from 1 to 20 msec, shown in the table. The total counting period is 10 to 200 msec. In the electric circuits the maximum counting rate is about 5×10^4 counts/sec. Thus the maximum counting rate is restricted not by a Ceratron multiplier but by the electrical circuits of data acquisition system. The signals stored in the memory cores are printed with a digital printer or a tape printer for on line data processing. In the present report all data

are obtained by off-line treatments of signals from the digital printer.

Table 1 Designed characteristics of 10-ch electrostatic energy analyser. X is a distance from the center of an incident slit to that of an exit slit, d distance between the deflecting and earth plates, dX_1 and dX_2 widths of the incident and exit slits, dV/V energy resolution, and h heights of the exit slits.

	X	d=90mm $\frac{2d}{X}$	dX_2	dX_1=5.92mm dV/V	h
CH 1	2.5 cm	7.20	6.76 mm	50.7 %	9.0 mm
CH 2	5.0	3.60	6.61	25.1	9.0
CH 3	7.5	2.40	6.63	16.7	9.0
CH 4	10.0	1.80	6.55	12.5	9.0
CH 5	12.5	1.44	6.12	9.63	9.0
CH 6	15.0	1.20	6.20	8.08	9.0
CH 7	17.5	1.02	8.05	7.98	10.0
CH 8	20.0	0.90	9.17	7.54	10.0
CH 9	22.5	0.80	10.92	7.48	11.0
CH 10	25.0	0.72	13.00	7.56	11.0

Table 2 Characteristics of smapling scalers for 10-ch neutral particle analysis.

sampling time	1, 2, 3, 4, 5, 6, 8, 10, 15, 20 msec
sampling number/ch	10
dead time	0.2 μsec at starting time, 0.5 μsec at sampling time
total counting period	10 msec --- 200 msec
maximum counting number/ch	9999

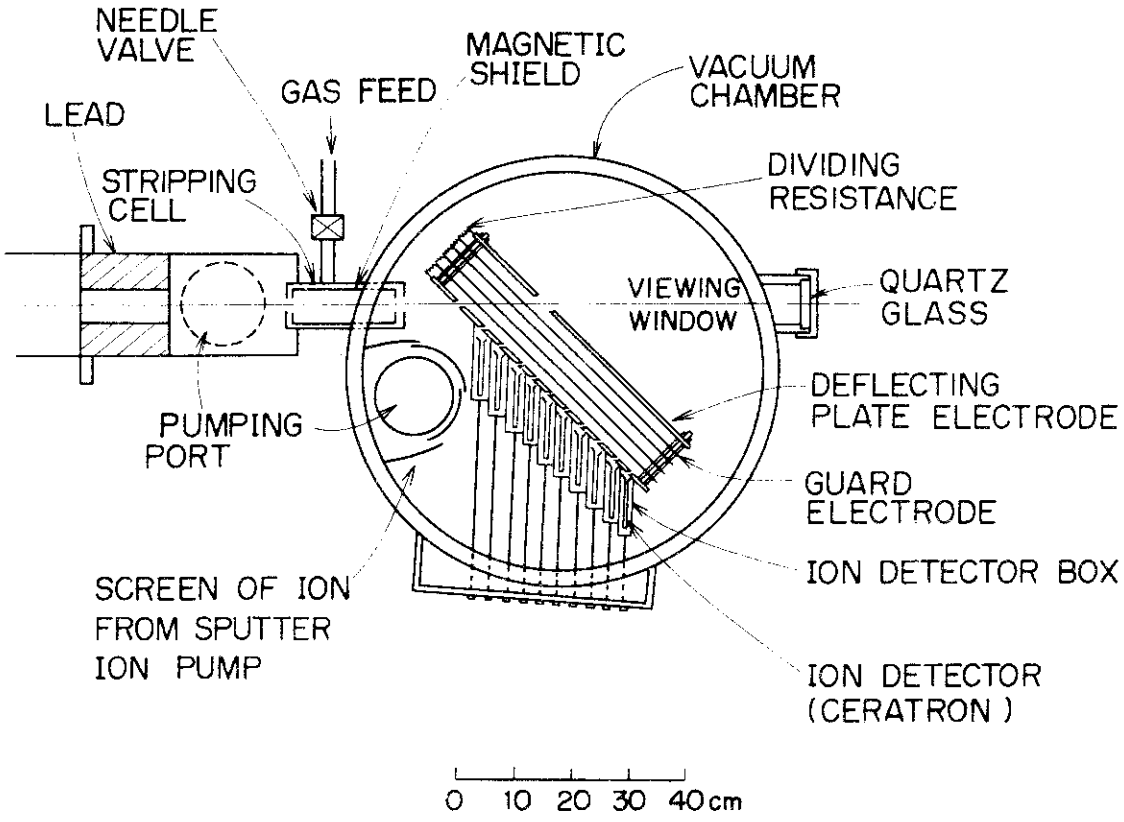

Fig. 1 Schematic diagram of 10-ch neutral particle energy analyser apparatus.

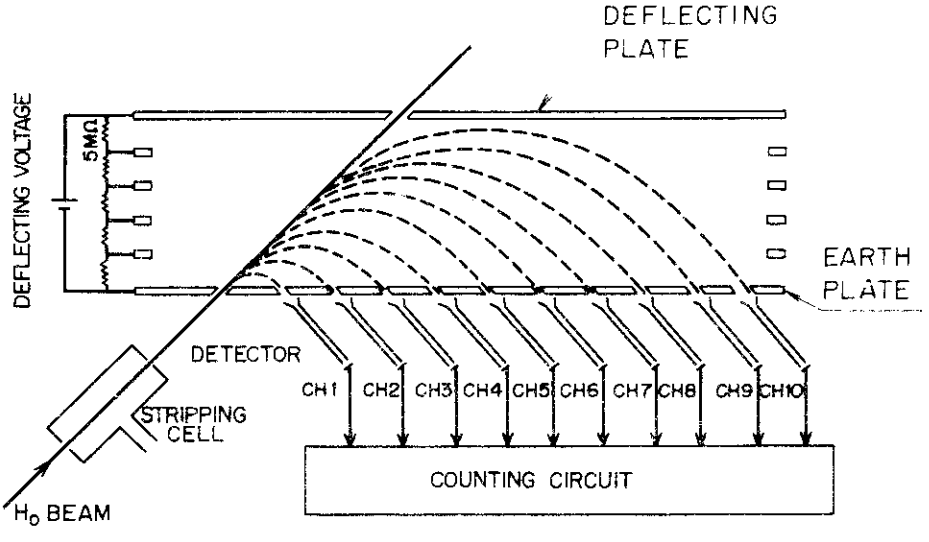

Fig. 2 Detailed drawing of an electrostatic energy analyser with ten ion detectors.

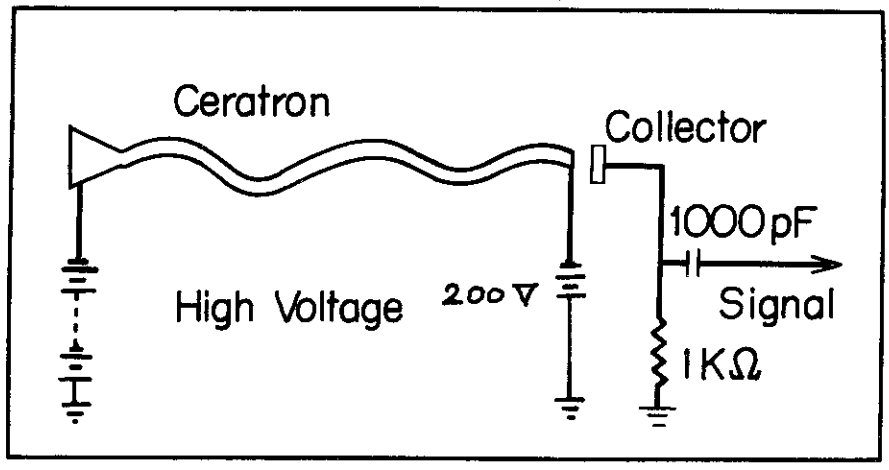

Fig. 3 Illustration of supplying a Ceratron multipler with voltages.

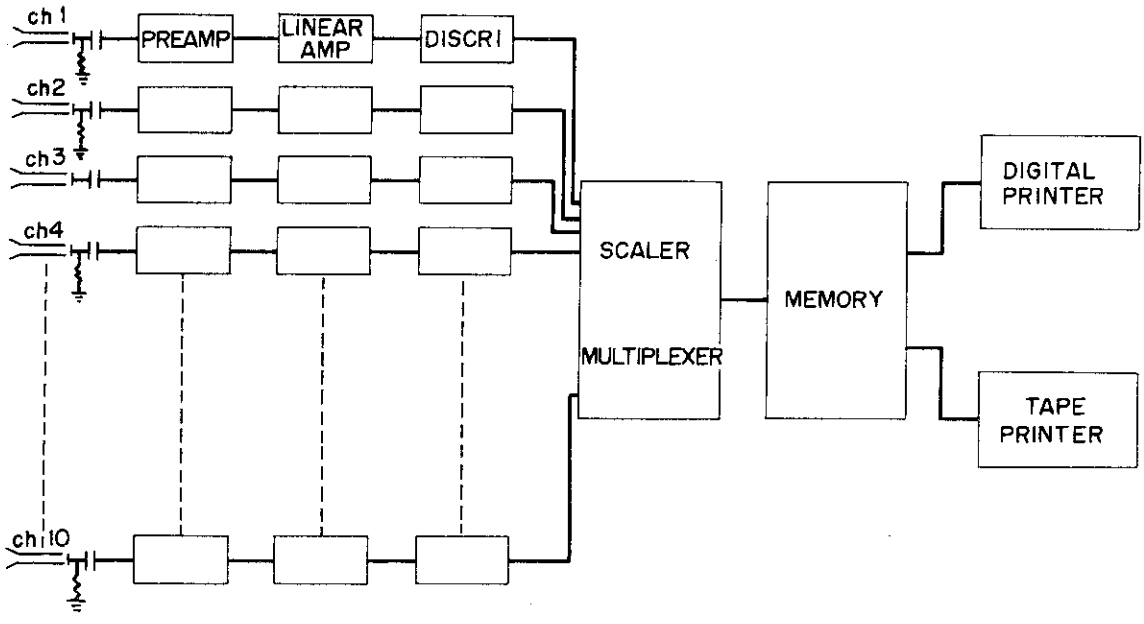

Fig. 4 Block diagram of pulse-counting circuits of data acquisition system for 10-ch particle analysis.

3. CALIBRATIONS OF ENERGY ANALYSER AND CHARGE STRIPPING EFFICIENCY

In order to determine ion temperatures from neutral particle analysis, three kinds of quantities which are presented below in this section are necessary to be calibrated or must be confirmed to be in sufficient agreement with the designed values. This section describes calibration experiments on the NPEAA. The schematic diagram of calibration experiments on the NPEAA is shown in Fig. 5.

The first step in calibration experiments is to confirm relations between an energy of the particles entering each channel and a deflecting voltage applied to the energy analyser, and to provide experimentally the energy resolutions. Energy calibrations are performed with an electron gun installed in front of an entrance slit S_3 of the charge stripping cell in Fig. 5.

The first step in calibration experiments is to confirm relations between an energy of the particles entering each channel and a deflecting voltage applied to the energy analyser, and to provide experimentally the energy resolutions. Energy calibrations are performed with an electron gun installed in front of an entrance slit S_3 of the charge stripping cell in Fig. 5. Other parts of an ion source, a charge exchange cell and a charged-particle deflector are removed, and any gases are not fed into a charge stripping cell. The profiles of output currents in each channel are obtained by scanning the deflecting voltage while the accelerating voltage of electron gun is kept constant. Faraday cups are used to detect the output electron currents. Figures 6(a) and (b) show the profiles in each channel plotted against the deflecting voltage for different values of electron energy. In these figures the profiles in ch-4 to ch-10 are for electron energies of 200, 400, 600, 800 and 1000 eV, the profile in ch-3 for 200, 300, 400, 500 and 750 eV, the profile in ch-2 for 200, 300, 400, 500 and 600 eV, and in ch-1 for 100, 200 and 300 eV. Figure 7 shows relations between the deflecting voltage and incident energy, which are deduced from Figs. 6(a) and (b). From Fig. 7 and Eq. (1), an experimental value of 2d/X can be determined for each channel. Table 3 shows comparisons for each channel between the design values (shown already in Table 1) and the experimental values of 2d/X. It is confirmed that the agreement between the experimental and designed values are fairly good within difference of 2 -- 5 percents. The difference appears to become larger, as the channel number increases. These circumstances may imply that there seems to be a

a slight distortion in the electric field of the energy analyser. However the difference of a few percents only produce negligibly small errors in determing ion temperatures. Energy resolutions of individual channels are estimated from Figs. 6(a) and (b). The experimental values of energy resolutions are listed in Table 4 for comparisons with the designed values of total signal width$(dV/V)_D$ (shown already in Table 1). Two kinds of experimental values obtained from Figs. 6(a) and (b) are indicated in the table, one referring to the enrgy resolution of full half-width $(dV/V)_{FHW}$ and another to the energy resolution of total signal width $(dV/V)_{TSW}$. The values of $(dV/V)_{TSW}$ accord remarkably with the designed ones except for ch-5, 6 and 7. Even for these channels disagreement between experiments and designs are only 10 -- 20 percents. More differences between $(dV/V)_D$ and twice of $(dV/V)_{FHW}$ observed for ch-7 to ch-10 are due to the fact that the widths of the exit slits (dX_2) are much larger than the diameter of an incident beam, which is limited by the width of the incident slit(dX_1).

Table 3 Comparisons between designed and experimental values of the factor 2d/X in Eq. (1).

ch		1	2	3	4	5	6	7	8	9	10
2d/X	designed	7.20	3.60	2.40	1.80	1.44	1.20	1.02	0.o0	0.80	0.72
	experimental	7.37	3.46	2.35	1.78	1.42	1.18	1.00	0.88	0.77	0.68

Table 4 Comparisons between designed and experimental values of energy resolutions. $(dV/V)_D$ is the designed resolutions, and $(dV/V)_{FHW}$ and $(dV/V)_{TSW}$ are experimental resolutions of full half width and of total signal width.

ch	1	2	3	4	5	6	7	8	9	10
$(dV/V)_D$	50.7%	25.1	16.7	12.5	9.63	8.08	7.98	7.54	7.48	7.56
$(dV/V)_{FHW}$	25.0%	12.8	8.76	6.60	4.20	4.20	4.44	4.46	4.76	5.26
$(dV/V)_{TSW}$	51.6%	27.5	16.7	11.6	8.03	9.63	7.29	7.30	7.48	7.65

The next step to calibrate the NPEAA is to measure a transmission efficiency of particles. In these measurements, the dependence of the transmission efficiency on the particle energy and the channel are investigated by using a proton beam. The experiments are performed in an experimental stand shown in Fig. 5, where however the charge exchange cell and charge stripping cell are evacuated and no gases are fed into them. The proton beams with energy of 1, 2 and 3 keV are separated with a 60-degrees momentum mass analyser from the hydrogen ion beam (H^+, H_2^+, H_3^+)

which is produced in an RF ion source. The proton beams are directly introduced to the incident slit of the energy analyser. A current of the proton beam flowing straightly through the energy analyser I_S is measured with a Faraday cup placed behind a hole of the deflecting plate when no voltage is applied to it. The output currents of the deflected proton beam I_C are measured with Faraday cups placed behind the exits of individual channels by scanning the deflecting voltage. In current measurements with a Faraday cup, secondary electrons emitted from a collector by the indicent proton beam are suppressed by a biased grid and the protons reflected at the collector are measured from currents flowing to the grid. Figure 8 shows the transmission efficiency I_C/I_S in each channel for different proton energies. Because of the shadow masks installed in front of the exit slits, the efficiencies are about 50 percents for all channels. It is confirmed from the figure 8 that the transmission efficiencies of particles are almost independent of the incident particle energy and the channel of the energy analyser.

The third step in calibrations is to examine the conversion efficiency in the charge stripping cell. Up to now the nitrogen gas has been used for a target gas in the charge stripping cell of a single-channel neutral particle energy analyser.[12] The conversion efficiency for nitrogen gas has already been calibrated. The results have shown that the measured values in the particle energy 400 eV are consistent with the theoretical ones calculated from cross-sections of the charge stripping and electron capture process in the charge stripping cell.[13] In the present report, hydrogen is adopted as a target gas and its stipping cell efficiency is investigated. The hydrogen gas is preferable to nitrogen with respect to a possibility of resulting impurity-influx, because the operating gas is mainly hydrogen in JAERI-tokamak devices.

Measurement of the conversion efficiency in the charge stripping cell is performed in a similar way which was conventionally used.[7,9,13] In Fig. 5, the proton beam produced by an RF ion source through a mass analyser is converted to an atomic hydrogen beam by colliding with H_2 gas which is stored at a pressure of about 10^{-4} torr in the charge exchange cell. The residual protons appearring behind the charge exchange cell are removed with a charged-particle deflector. The intensity of the atomic beam F_0 is determined from measurements of secondary electrons with a Faraday cup placed behind a hole of the deflecting plate, without feed of gases into the charge stripping cell, by assuming that the secondary electron

emission coefficient for a atomic hydrogen beam is the same as that for a proton beam. The charge stripping cell has a length of 20 cm, a diameter of 4 cm and the apertures of an incident and exit slits are 4 mm in diameter. The atomic hydrogen beam collides with H_2 gas fed into the charge stripping cell whose pressure is a few 10^{-4} torr, and resulting stripped-ions are separated from the atomic hydrogen beam in the energy analyser. The intensity of the stripped-ion beam F_1 is also measured with a Faraday cup placed behind an exit slit corresponding to the beam energy. Since the measured value of F_1 is the intensity of ion beam which passes through a shadow mask, the real intensity of the stripped-ion beam F_1' can be determined by correcting the F_1-value by the transmission efficiency shown in Fig. 8. Thus the conversion efficiency in the charge stripping cell is determined from the ratio of F_1' to F_0. Experiments to calibrate the conversion efficiency in the cell are performed for $p\ell$ = 0.048 torr·cm to the hydrogen atom beams with energy of 2, 3 and 4 keV. The experimental results are shown in Fig. 9, where the measured conversion efficiencies indicated by open circles are compared with the charge stripping cell efficiencies which were theoretically calculated from cross-sections of the charge stripping and electron capture process by Koopman[16,17] and Allison[18] respectively.

The measured conversion efficiency in the charge stripping cell is in fairly good agreement with the theoretically calculated value in a range of 2 to 4 keV, as shown in Fig. 9. Recently Noda[15] pointed out that the experimental conversion efficiencies in hydrogen gas are in good agreement with the theoretically calculated values for particle energies higher than 300 eV and for a charge stripping cell of $p\ell$ = 0.02 torr·cm. In a previous report[13] the conversion efficiency calculated theoretically for nitrogen gas is confirmed to agree well with the experimental one in an energy range higher than 400 eV, as described previously. Thus it is plausible that the theoretical values also provide reasonable efficiencies for hydrogen gas in an energy range higher than 300 eV or 400 eV. In the present report, we adopt the theoretically calculated conversion efficiencies in determining ion temperatures of JAERI-tokamak devices with the 10-ch NPEAA, and we determine the values of ion temperatures from the spectrums of charge-exchanged, fast atoms observed in the energy range higher than 400 eV.

The validity of this assumption is more important particularly for the measurements on JFT-2a plasmas, which have ion temperatures of about a hundred eV. In order to confirm the justification of the assumption,

doppler broadening of Balmer H_α-line radiated from charge-exchanged hydrogen atoms is simultaneously observed for JFT-2a plasmas and are compared with the results from the analysis of charge-exchanged particles with 10-ch NPEAA. Some discussions on comparisons between charge-exchange and doppler measurements are presented in Section 6.

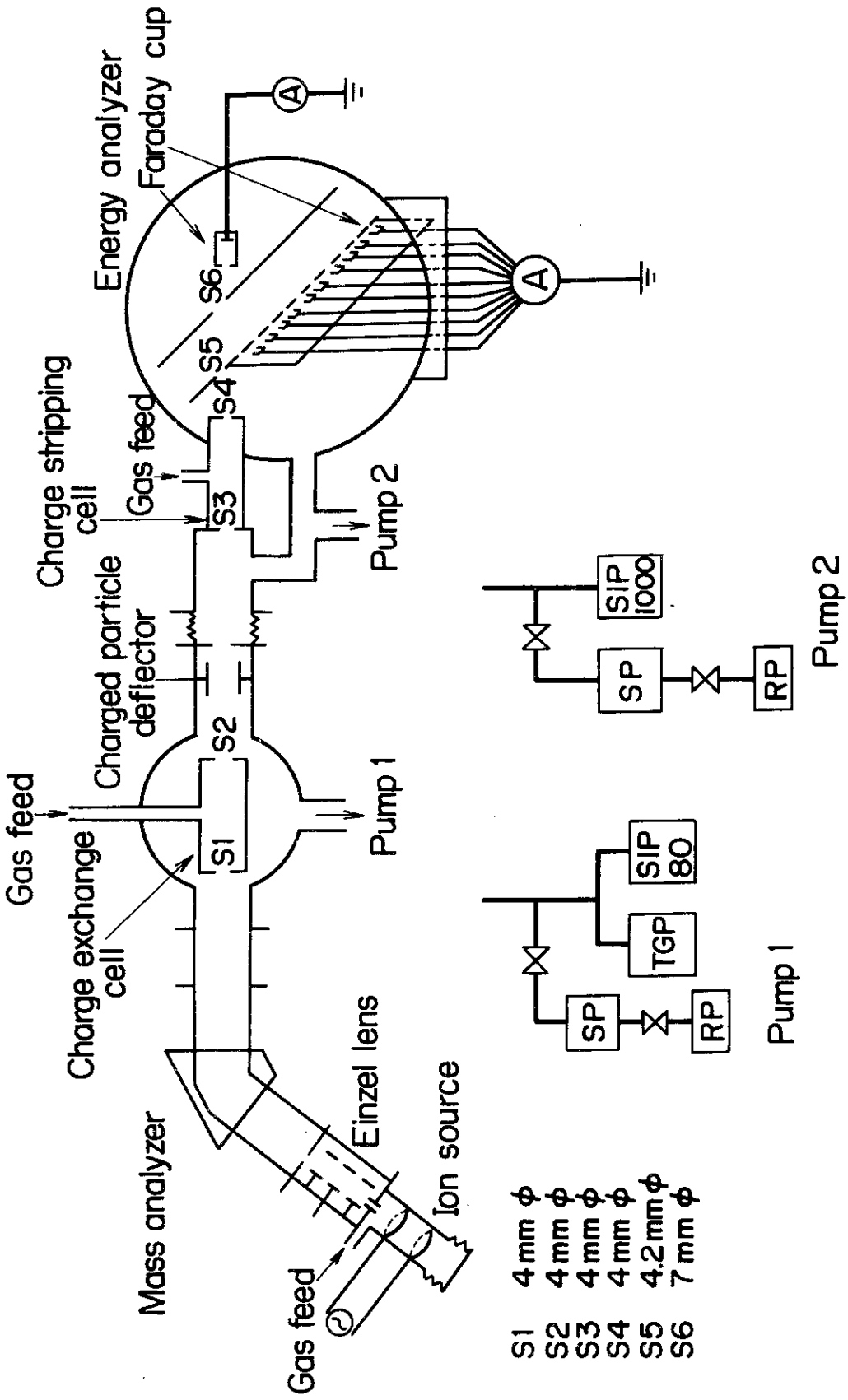

Fig. 5 Schematic diagram of the apparatus for calibration experiments.

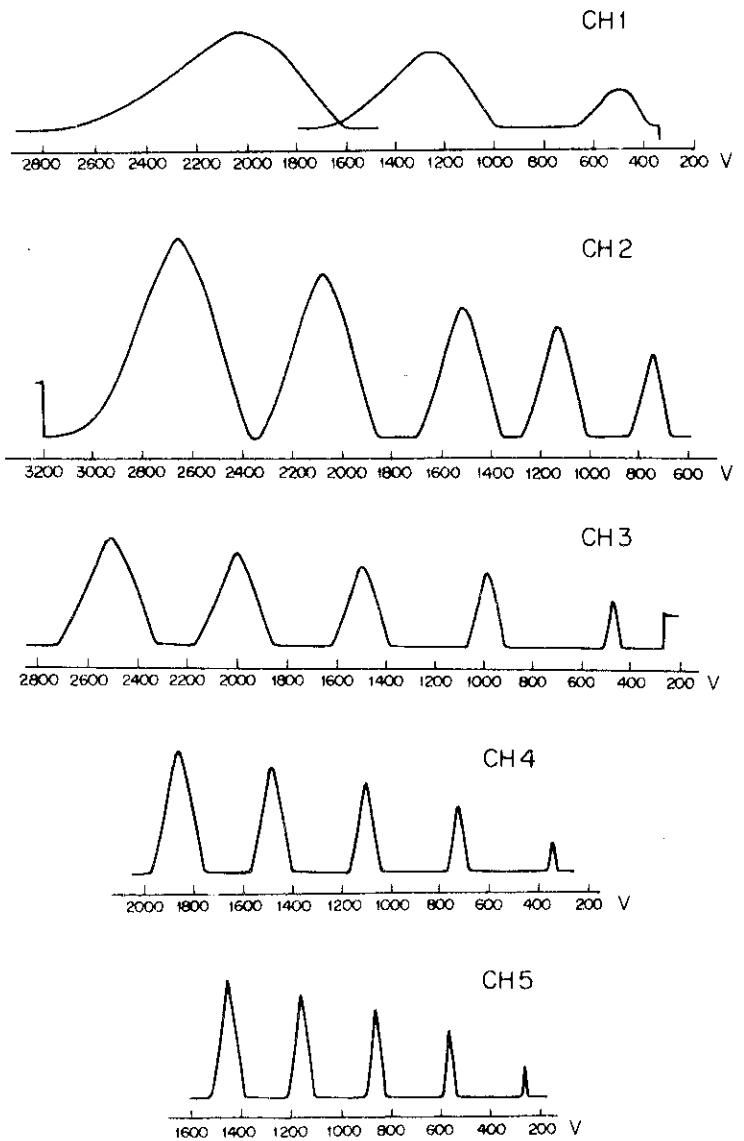

Fig.6(a) Output profiles for ch-1 to ch-5 of the energy analyser.

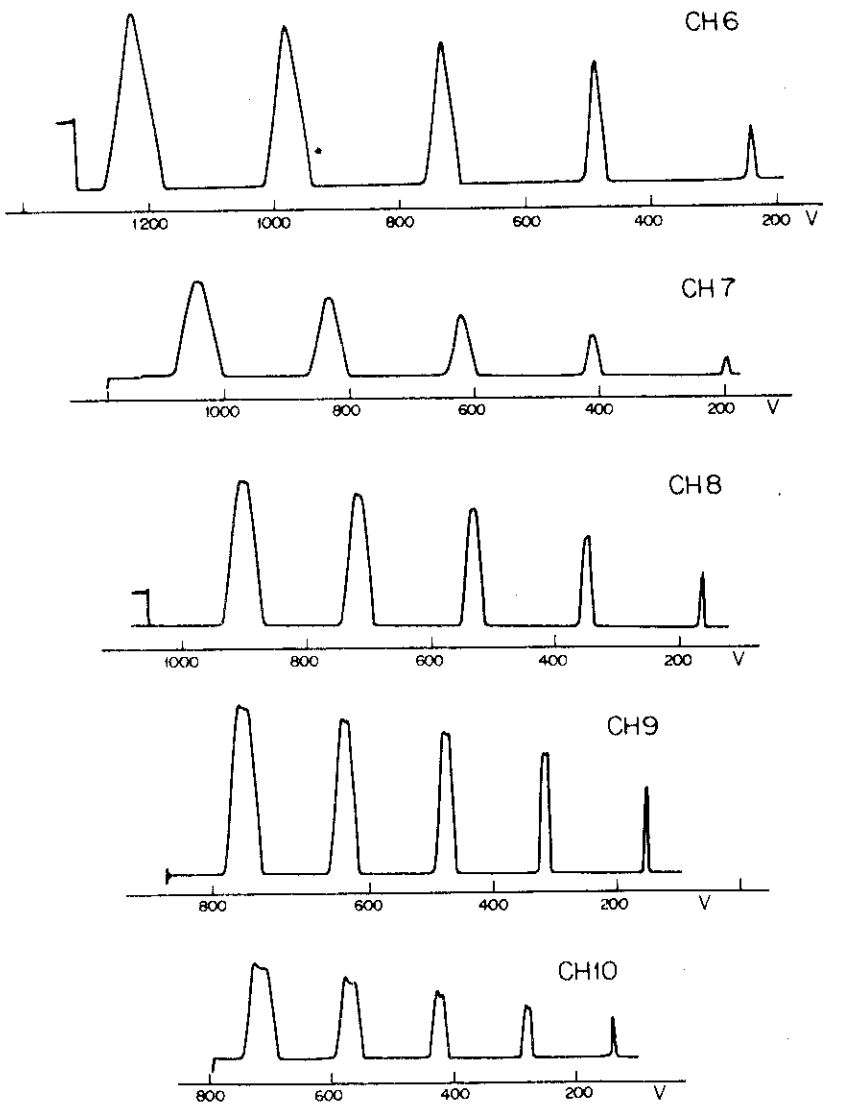

Fig.6(b) Output profiles for ch-6 to ch-10 of the energy analyser.

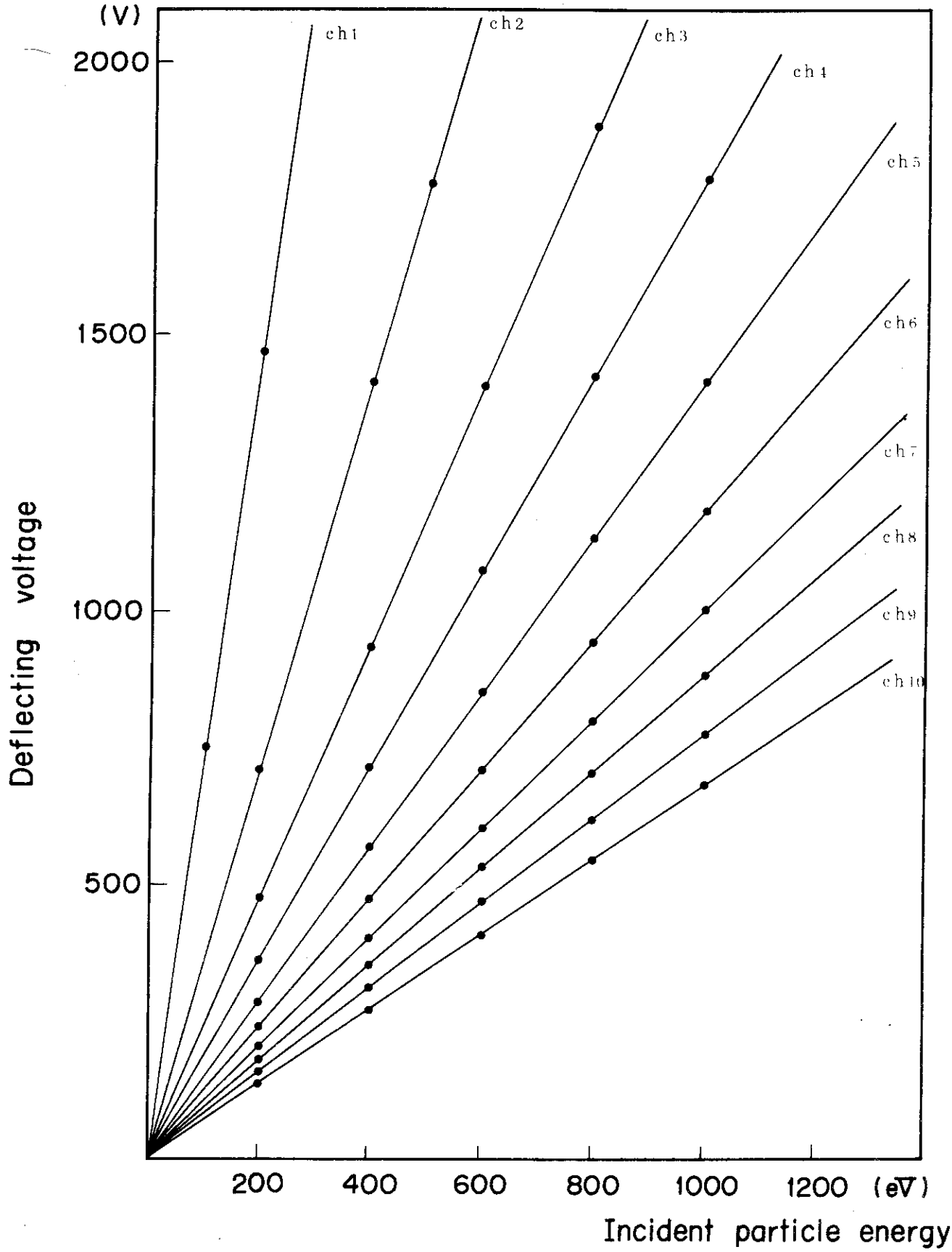

Fig. 7 Relations between the deflecting voltage and the incident particle energy.

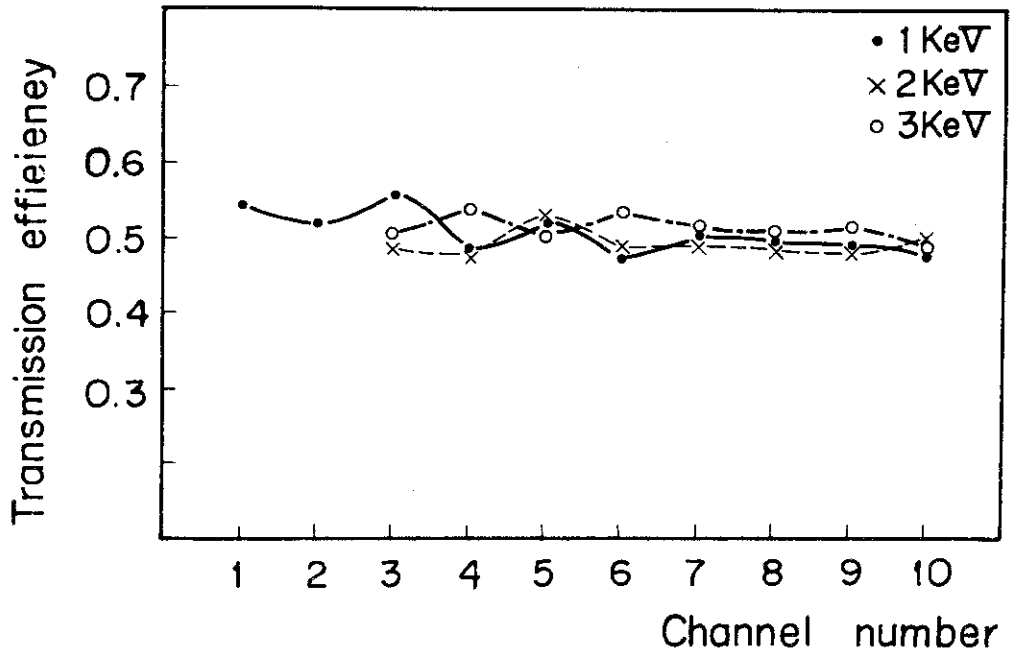

Fig. 8 Transmission efficiency of protons in each channel for different energies.

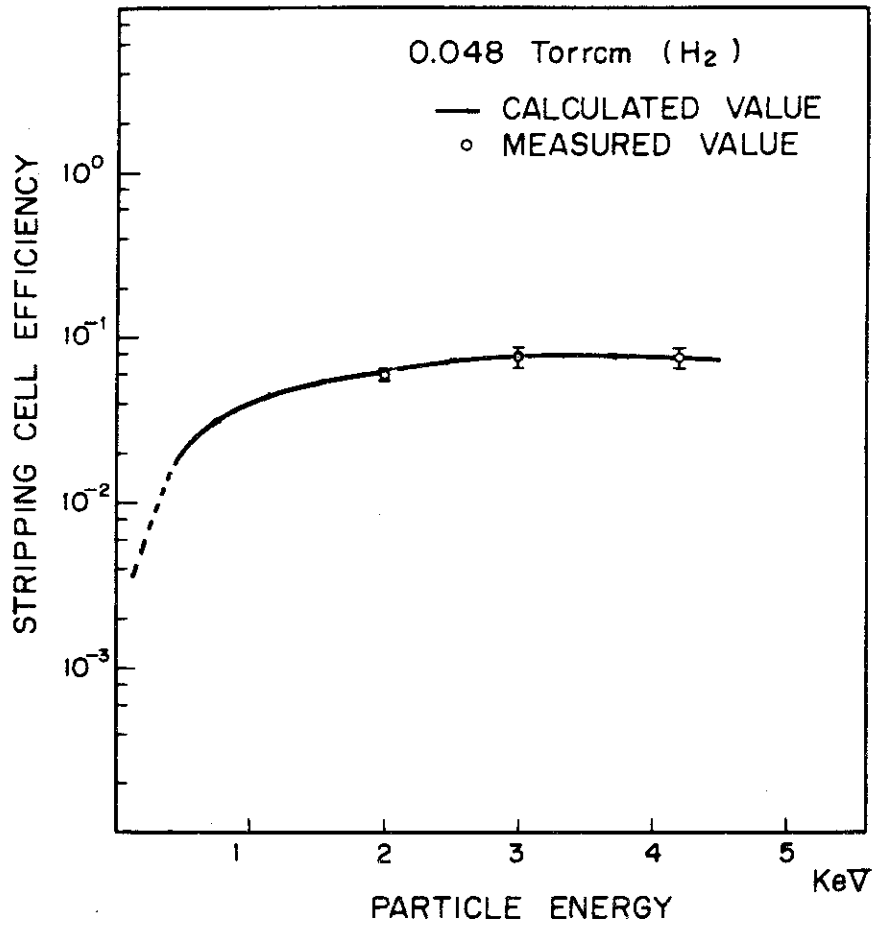

Fig. 9 Conversion efficiency in the charge stripping cell filled with H_2 gas.

4. EXPERIMENTAL ARRANGEMENTS OF NEUTRAL ANALYSIS AND RESULTS OF ION TEMPERATURE MEASUREMENTS ON JFT-2a AND JFT-2 PLASMAS

Measurements of ion temperatures with the 10-ch NPEAA are performed on JFT-2a[19] (a non-circular cross-section tokamak) and JFT-2[20] (a fat, circular cross-section tokamak) devices. The main machine parameters of these tokamak devices are shown in Table 5. The present paper is the first report which describes the measurements of ion temperatures on JFT-2a device and on JFT-2 device with the toroidal magnetic field being upgraded from 10 kGauss to 18 kGauss. Before upgrading the ion temperatures of JFT-2 plasma were measured with a single-channel neutral energy particle analyser.[12,20]

Table 5 Main features of JAERI-tokamad devices, JFT-2a and JFT-2.

	JFT-2a[19]	JFT-2[20]
major radius	60 cm	90 cm
minor radius	∿10 cm	25 cm
maximum toroidal magnetic field	10 kGauss	18 KGauss
remark	noncircular cross-section tokamak with a divertor	fat, circular cross-section tokamak with a dynamic limiter

The experimental set-up for measuring ion temperatures is shown in Fig. 10. A photograph of 10-ch NPEAA connected to JFT-2a device is shown in Fig. 11. A drift pipe between the plasma device and the NPEAA is pumped out with a sputter ion pump whose pumping speed is 80 l/sec and a T_i-getter pump. The drift tube is electrically separated from the vacuum chamber of the plasma device to prevent spurious currents and noises due to plasmas from entering the detection system of NPEAA. Except when measurements are performed, the NPEAA is isolated from the plasma device with a gate value in vacuum. The energy analyser of the NPEAA is shielded from hard X-ray irradiations coming from plasmas with lead of 10 cm thickness so that they do not hit ion detectors, i.e., Ceratron multipliers. Consequently, the noises of ion detectors originated from hard X-rays can be reduced to negligibly small levels in temperature measurements. In addition, the analyser and stripping cell are also shielded magnetically with iron and metal materials of high permeability (permaloy) in order that ion orbits in them are not disturbed due to the poloidal magnetic fields

produced by plasma currents.(*) The magnetic shielded consists of two layers of permaloy and one layer of iron are installed outside a vacuum chamber of the energy analyser, and two layers of permaloy inside the charge stripping cell. The effectiveness of the magnetic shields was examined in case of 100 kAmp discharges in JFT-2 device. The spatial distribution of magnetic field in the energy analyser and the charge stripping cell is measured with a search coil. Results are indicated in Fig. 12, where an external stray field of 48 Gauss due to the plasma current is reduced down to less than 1.1 Gauss on the ion orbits inside the energy analyser. In the charge stripping cell the field strength is realized to be smaller than 1 Gauss. It is inferred from the orbit analysis[12] that such magnetic fields are too negligibly small to influence determination of ion temperatures. Thus there does not seem to be any problems on stray fields for plasma currents of a few 10 kAmp in JFT-2a device and a few hundred kAmp in JFT-2 device.

Photon fluxes from tokamak plasmas probably become main noise sources in the measurement of ion temperatures, since Ceratron multipliers seem to have similar sensitivities for ultra-violet radiations as Channeltron multipliers. As the analyser does not have any treatment to absorb the u-v photons, they are reflected at the wall of the vacuum chamber or the deflecting plate of the energy analyser. Then such reflected photons may enter the Ceratrons behind the earth plate. The ratios of signals to noises are typically of an order of ten, except in early periods of plasma formation stage, for the present measurements on JFT-2a plasmas and JFT-2 plasmas. Fairly good S/N ratios of about 50 can be realized for high-density operations in JFT-2 device.

Ion temperatures are determined by measuring the particle signals in a discharge and the back-ground noises in the following discharge in turn. The net number of particle signals for individual channels is obtained by substracting mean values of the back-ground noises from the particle signals in each plasma shot. The mean values of the back-ground noises are averaged over a few shots. The count number of particle signals to be detected is adjusted by controlling a pressure in the charge stripping cell. In the experiments the pressure is varied from 1 to 5×10^{-4} torr in H_2. Other parts of the energy analyser are constantly kept below 5×10^{-6} torr.

(*) The maximum leakaged stray field near a setting position of the analyser has known to be due to plasma currents for JFT-2a and JFT-2 devices.

The 10-ch NPEAA is connected to a port of JFT-2a device, horizontally and perpendicularly to the toroidal direction, at a position which is 135 degrees away from the limiter position clockwise in the toroidal direction. The port has a diameter of 30 mm and is in use for observing the plasma center horizontally. A light from a H_e-N_e gas laser is used for centering of the center of port, the slits of the charge stripping cell, the incident slit of the earth plate and hole the deflecting plate through aquartz window (see Fig. 1) behind the deflecting plate. In this section we show the measurements performed for typical hydrogen-plasmas in JFT-2a[19b], where the toroidal magnetic field is 10 kGauss, the peak plasma current 15 kAmp, the ratio of the divertor current to the plasma current 1.1, and the peak electron temperature from ruby laser scattering measurements 240 ± 50 eV. Figure 13 shows time-variation of averaged electron density along a vertical path at R = 60 cm (R:major radious) measured with a 4-mm wave interferometer as well as there of loop voltage, plasma current and divertor current. Charge-exchanged, fast hydrogen-atoms emitted from the plasma and introduced to the drift tube are ionized in the stripping cell and analysed in the energy analyser of 10-ch NPEAA. Time-variations of net count number of particles entering individual channels are shown in Fig. 14, where the energy corresponding to each channel is also presented. These data are observed for the deflecting voltage 600 eV and the sampling time 3 msec. The number of plasma protons for each energy is deduced by dividing the net particle signals (shown in the figure) by the correction factors including the energy resolution, the transmission efficiency of particles (shown in Fig. 8), the conversion efficiency in the charge stripping cell (shown in Fig. 9 for $p\ell$ = 0.048 torr·cm) and the cross-section of resonance charge exchange process. The spectrums of the protons in a semi-logarithmic scale are shown in Fig. 15(a) and (b) at times (6 -- 9) msec and (9 -- 12) msec after the breakdown, respectively. The energy spectrums can be determined from particle signals in three shots and the mean back-ground noises averaged over the other three shots, that is, totally from six-shot discharges. The error bars indicated in these spectrums are the breadths estimated by assuming that the particle signals accord with a student-distribution of three samples and 90-percents reliability. The spectrums in an energy range higher than 400 eV, indicated by the solid lines, give ion temperatures of 87 eV and 113 eV. According to the discussions, mentioned in section 3, on the conversion efficiency in the charge stripping cell, the data below 400 eV, which are shown by

the dotted lines do not seem to be reliable. In order to discuss the spectrums in the lower energy range, it is necessary to calibrate the conversion efficiency in the stripping cell for this energy range.

In Fig. 16 the time-variation is shown of the ion temperature for the JFT-2a plasma. The bars of the experimental values indicate the maximum scatters in several measurements performed under the same operating conditions. As mentioned before one measurement needs six shots to determine the ion temperature. The peak ion temperature is 120 ± 15 eV at the time 9--12 msec after the breakdown. It is seen in Fig. 14 that this time of the peak temperature coincides with the time when the maximum particle numbers are observed to emit from the plasma for higher energy channels.

On JFT-2 plasmas, the measurements with 10-ch NPEAA are performed at a position of 135 degrees distant from a fixed limiter counter-clockwise in the toroidal direction. The results are described for the plasma obtained under the toroidal field 14 kGauss and the maximum current 100 kAmp. Figure 17 shows time-variations of plasma current, loop voltage, and mean electron density averaged along the central vertical path (at R = 90 cm). Time-variations of net particle numbers in individual channels observed for the deflecting voltage 1400 V and the sampling time 10 msec are shown in Fig. 18. Energy spectrums of protons in a semi-logarithmic scale are shown in Fig. 19(a) and (b). These data were obtained from three shots for particle signals and three shots for back-ground noises, i.e., only six shots, and the ion temperature can be determined by the same procedure as shown in Fig. 15 for JFT-2a. In Fig. 19(a) and (b), however, the data for ch-6 and ch-8 corresponding to 1166 eV and 1554 eV are omitted, because gains of Ceratrons for these two channels, reduced to about 1/10 in comparison with their regular values. The energy spectrums for higher than 400 eV are in good agreement with Maxwellian distributions which give ion temperatures of 278 eV and 347 eV at the time 20 -- 30 msec and 30 -- 40 msec, respectively.

The time-variation of ion temperatures for the JFT-2 plasma is shown in Fig. 20, where the bars show the maximum scatters in several measurements obtained on the same assumption as in Fig. 16. The plasma shots of 42 discharges are required to obtain the data in Fig. 20. It is shown from this figure and Fig. 18 that the peak ion temperature of 270 ± 80 eV is realized at 35 msec(*) when the maximum particle numbers are observed in

(*) Strictly sreaking, the value of ion temperature is realized at the sampling time of 10 msec from 30 to 40 msec.

channels except ch-1. Simultaneous measurements of ruby laser scattering show the central electron temperature of 490 ± 50 eV at that time.[22] At an initial stage of plasma formation before 10 msec, the S/N ratio is observed to be about unity for each channel and the ion temperature cannot be determined.

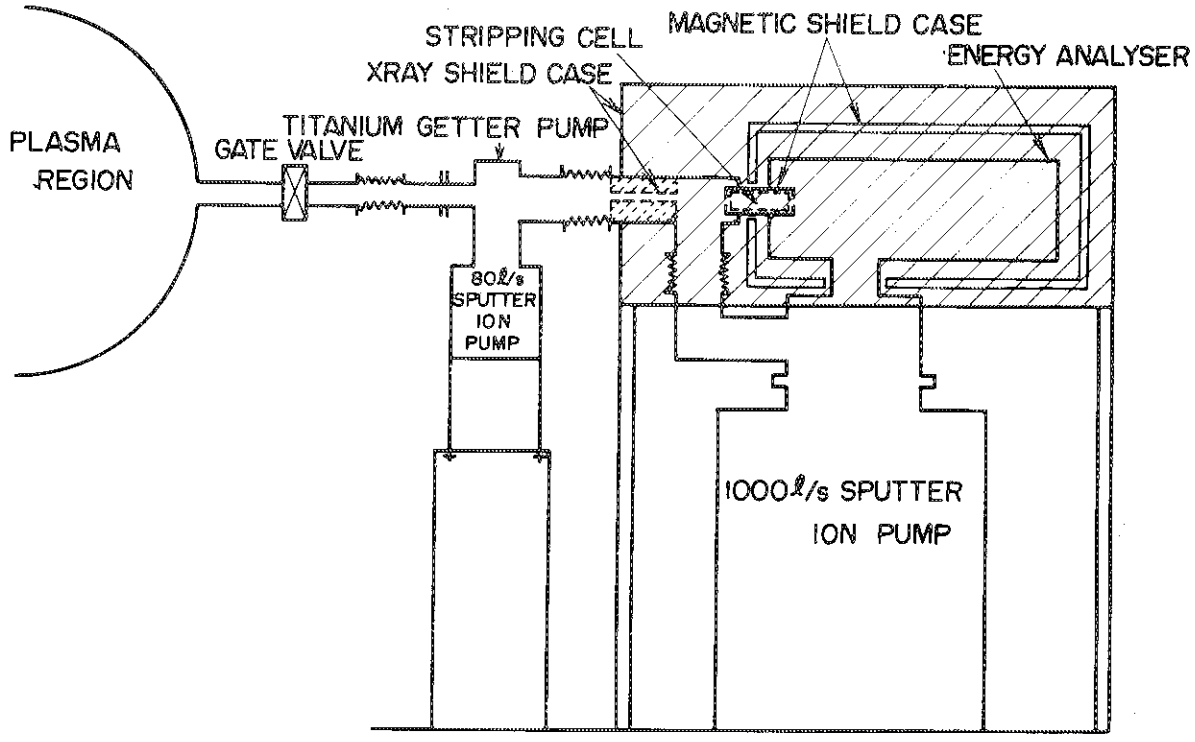

Fig. 10 Experimental set-up for measuring ion temperatures of JAERI-tokamak plasmas.

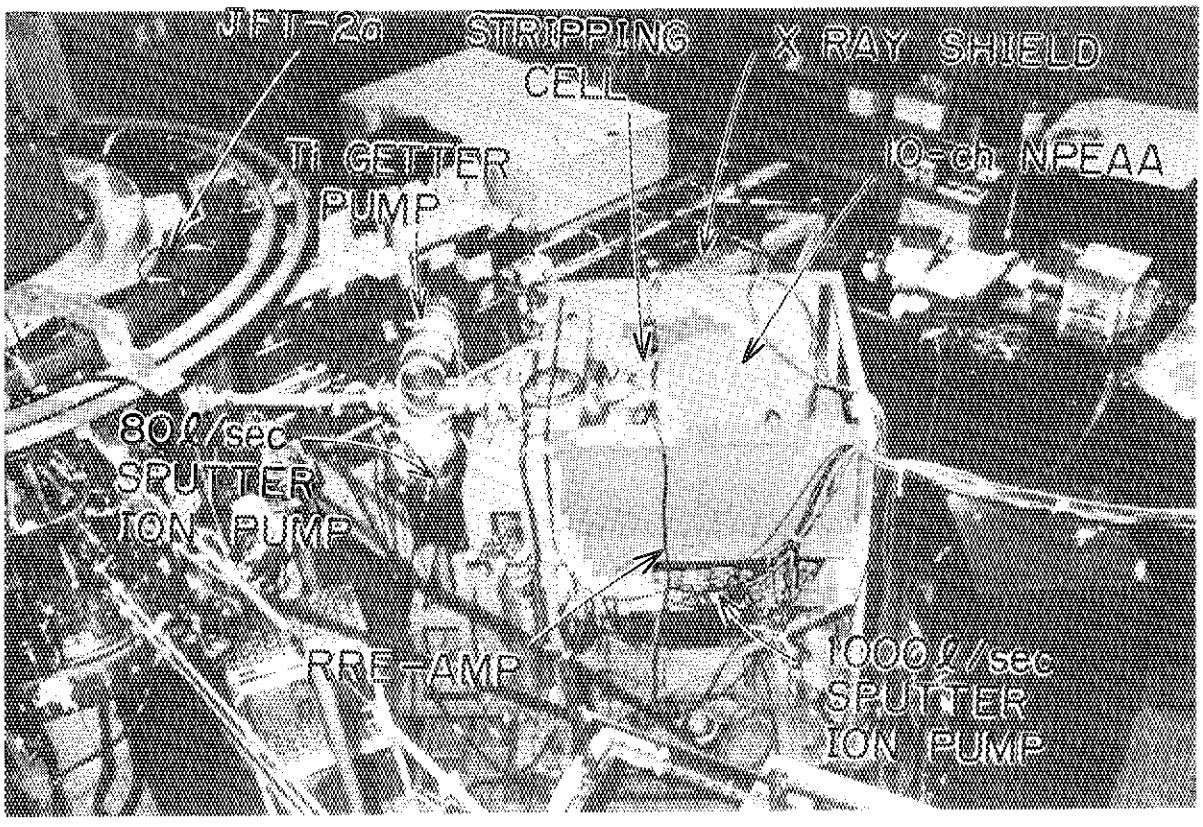

Fig. 11 Photograph of the neutral particle energy analyser apparatus connected to JFT-2a device.

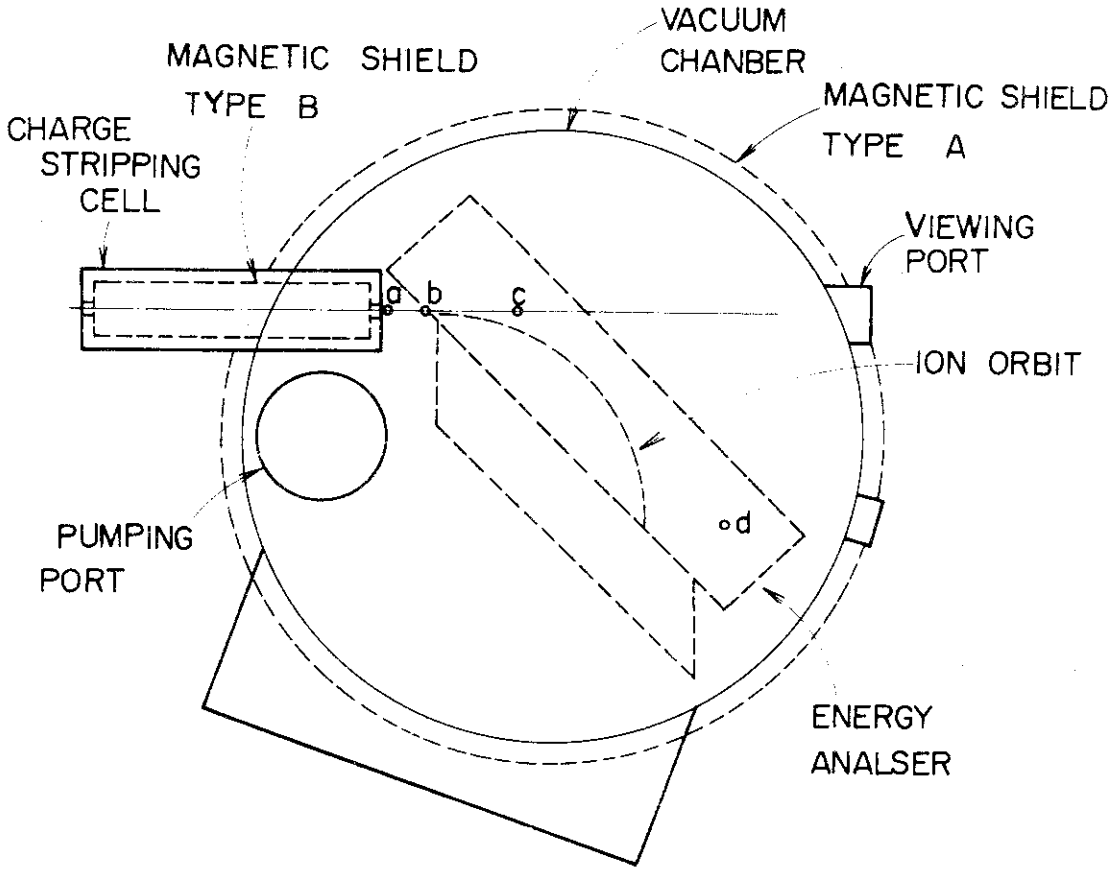

POSITION	MAGNETIC FIELD	
a	1.1	GAUSS
b	0.95	〃
c	0.78	〃
d	0.76	〃

PLASMA CURRENT : 100 KA

Fig. 12 Strength of leakaged stray magnetic fields in the energy analyser shielded magnetically.

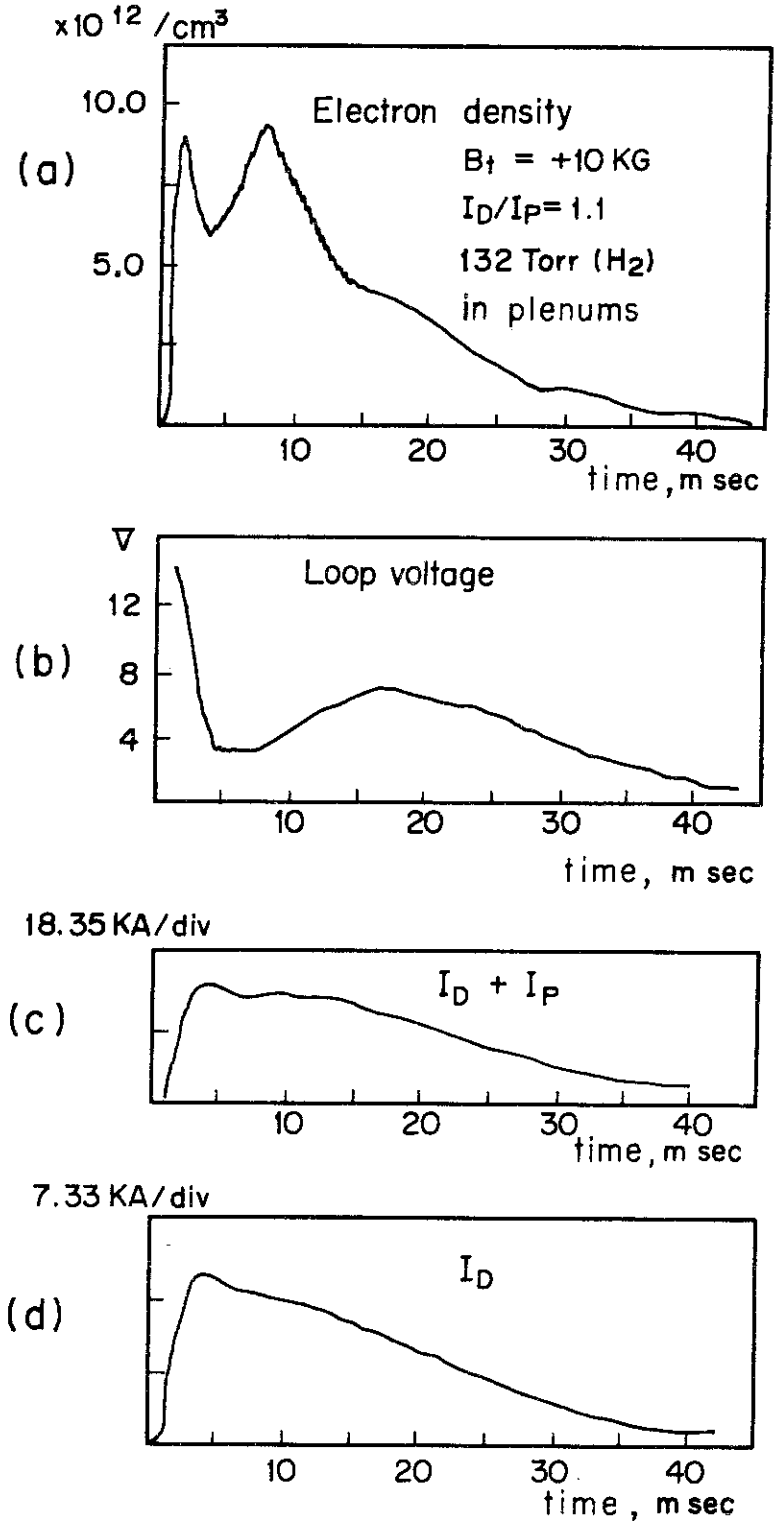

Fig. 13 Time-variations of main plasma parameters for the typical JFT-2a plasma.
(a) average electron density, (b) loop voltage, (c) divertor current I_D + plasma current I_p, and (d) divertor current I_D

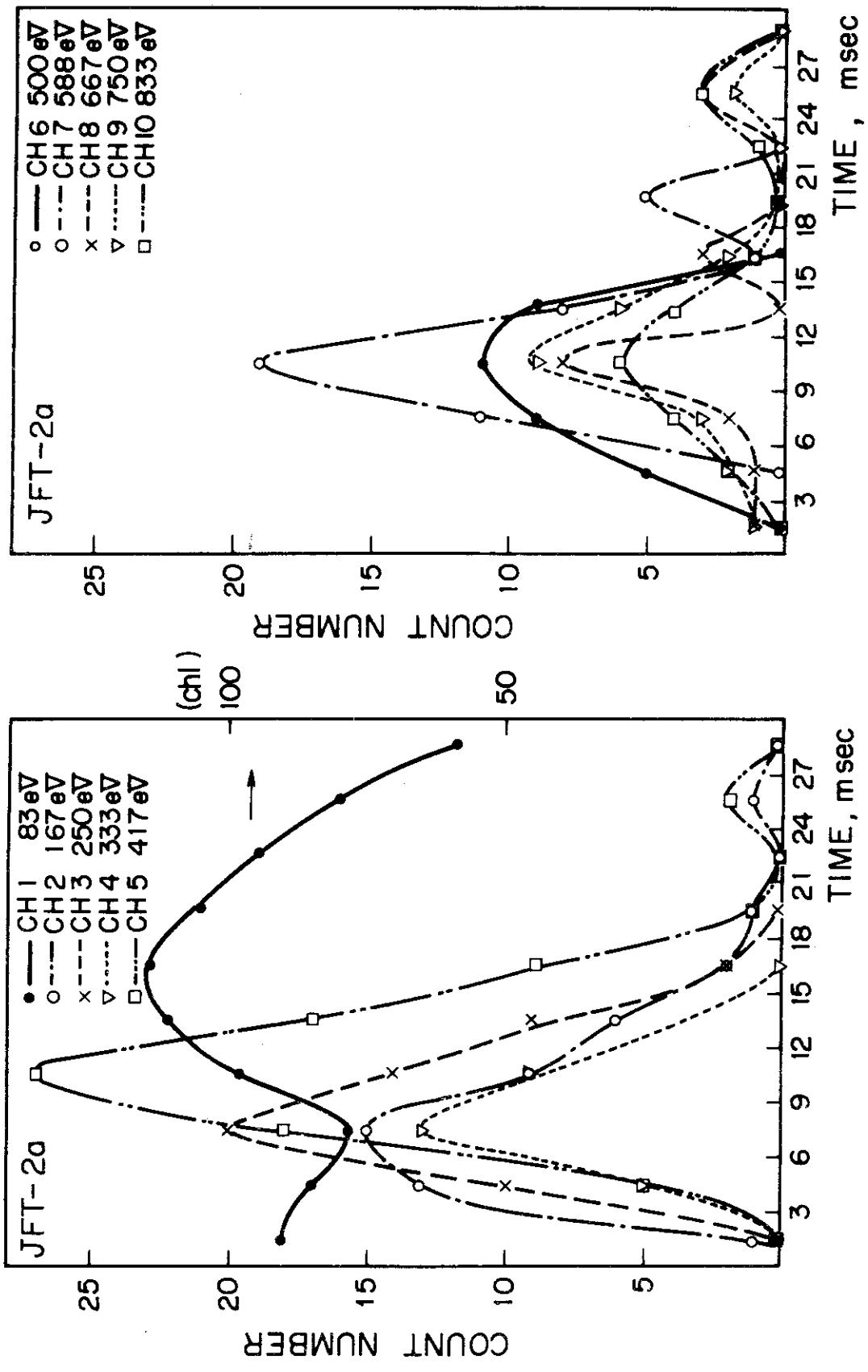

Fig. 14 Time-variations of net numbers of particles entering into individual channels for the JFT-2a plasma.

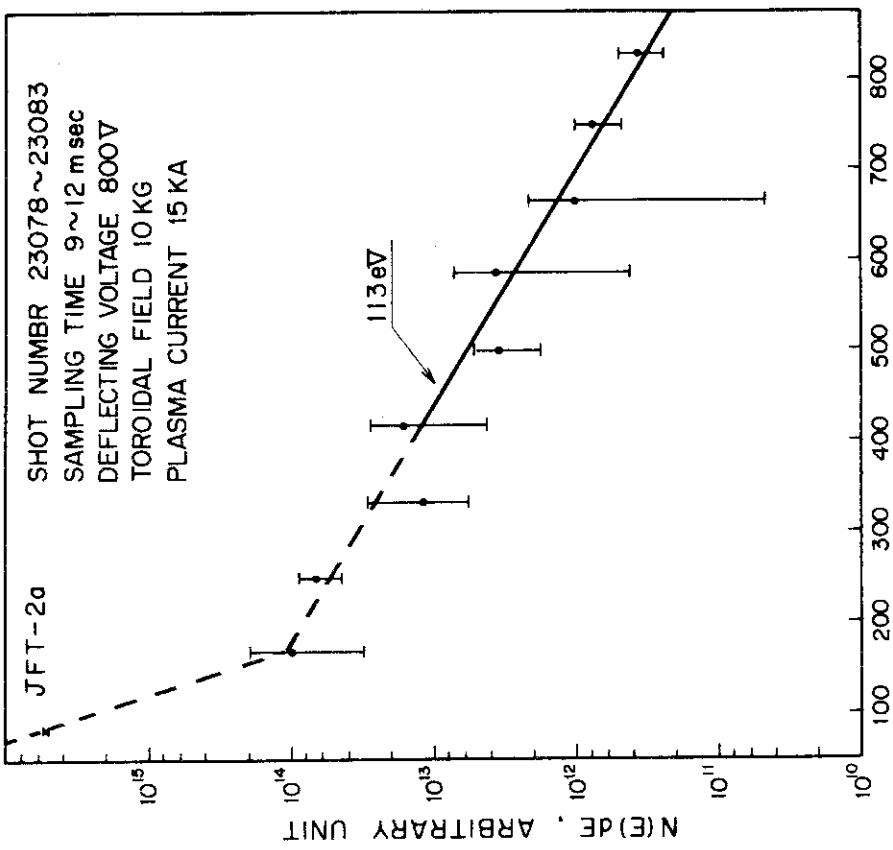

Fig.15(b) Proton energy spectrum observed on the JFT-2a plasma at 9 -- 12 msec after a breakdown.

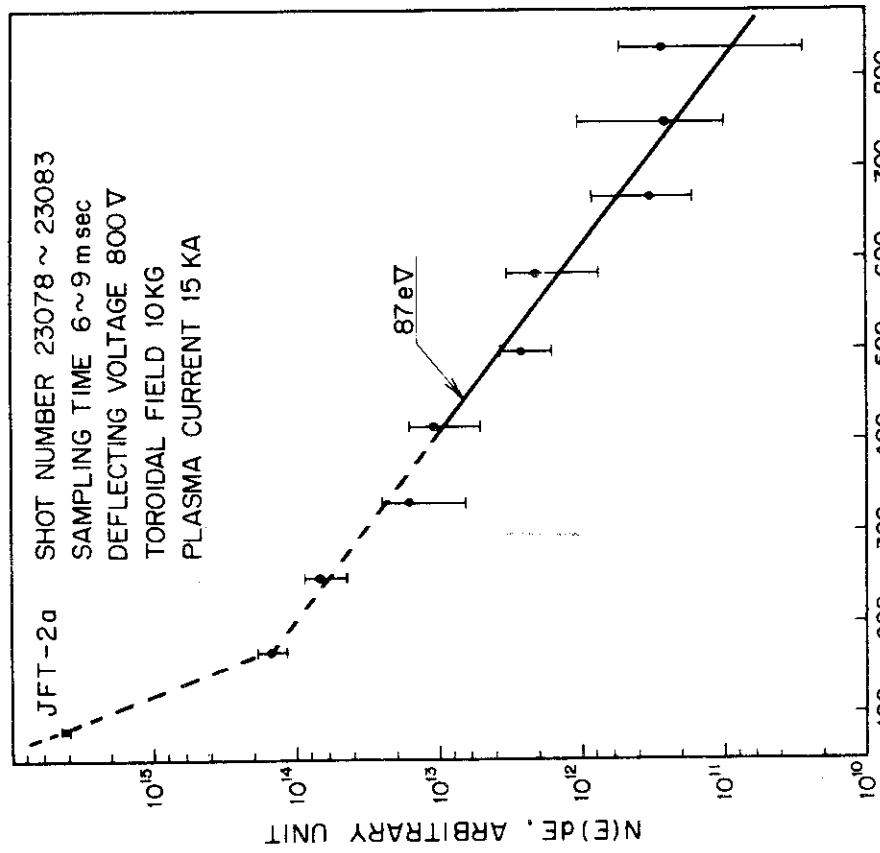

Fig.15(a) Proton energy spectrum observed on the JFT-2a plasma at 6 -- 9 msec after a breakdown.

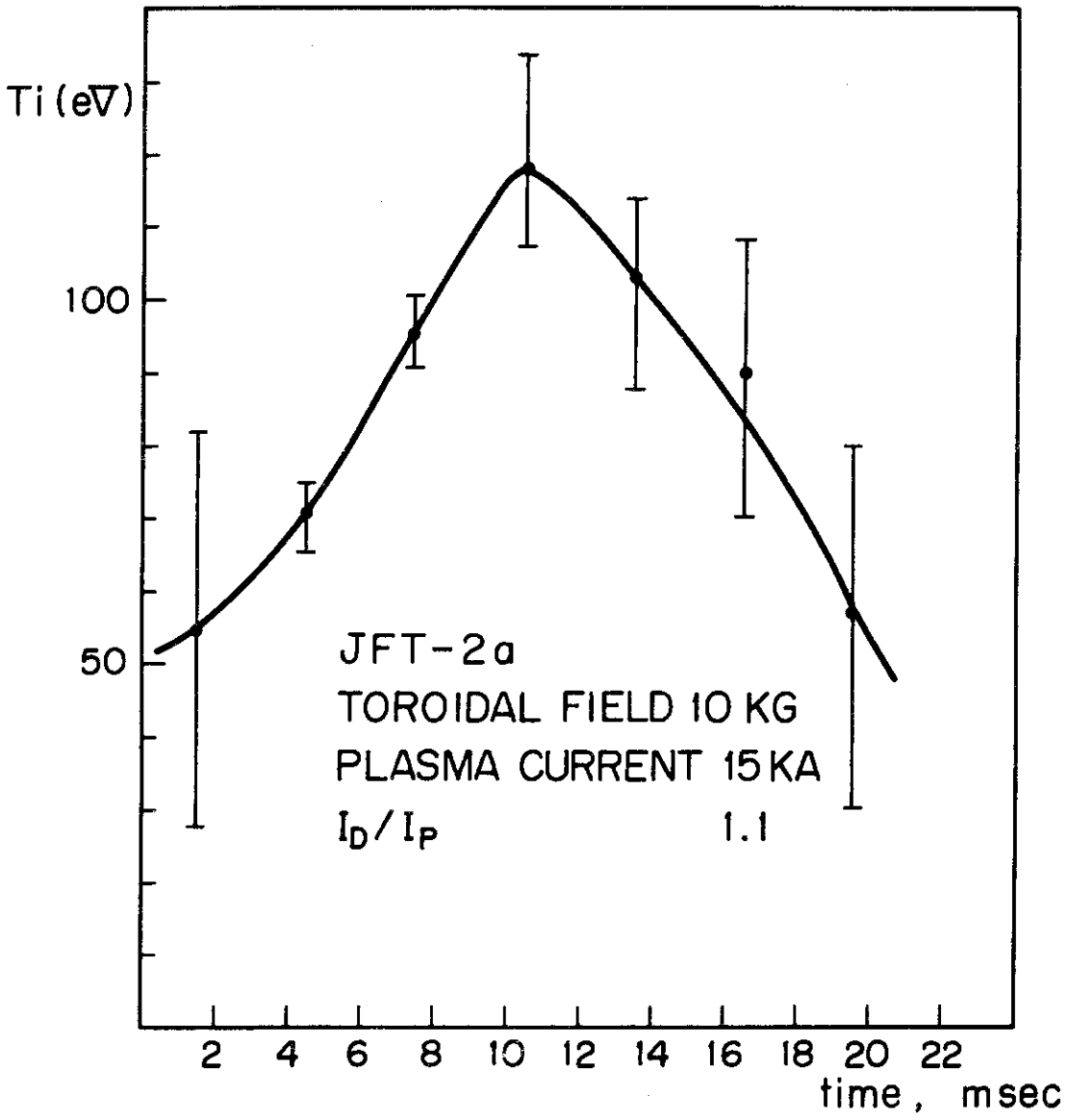

Fig. 16 Time-variations of ion temperature for the JFT-2a plasma.

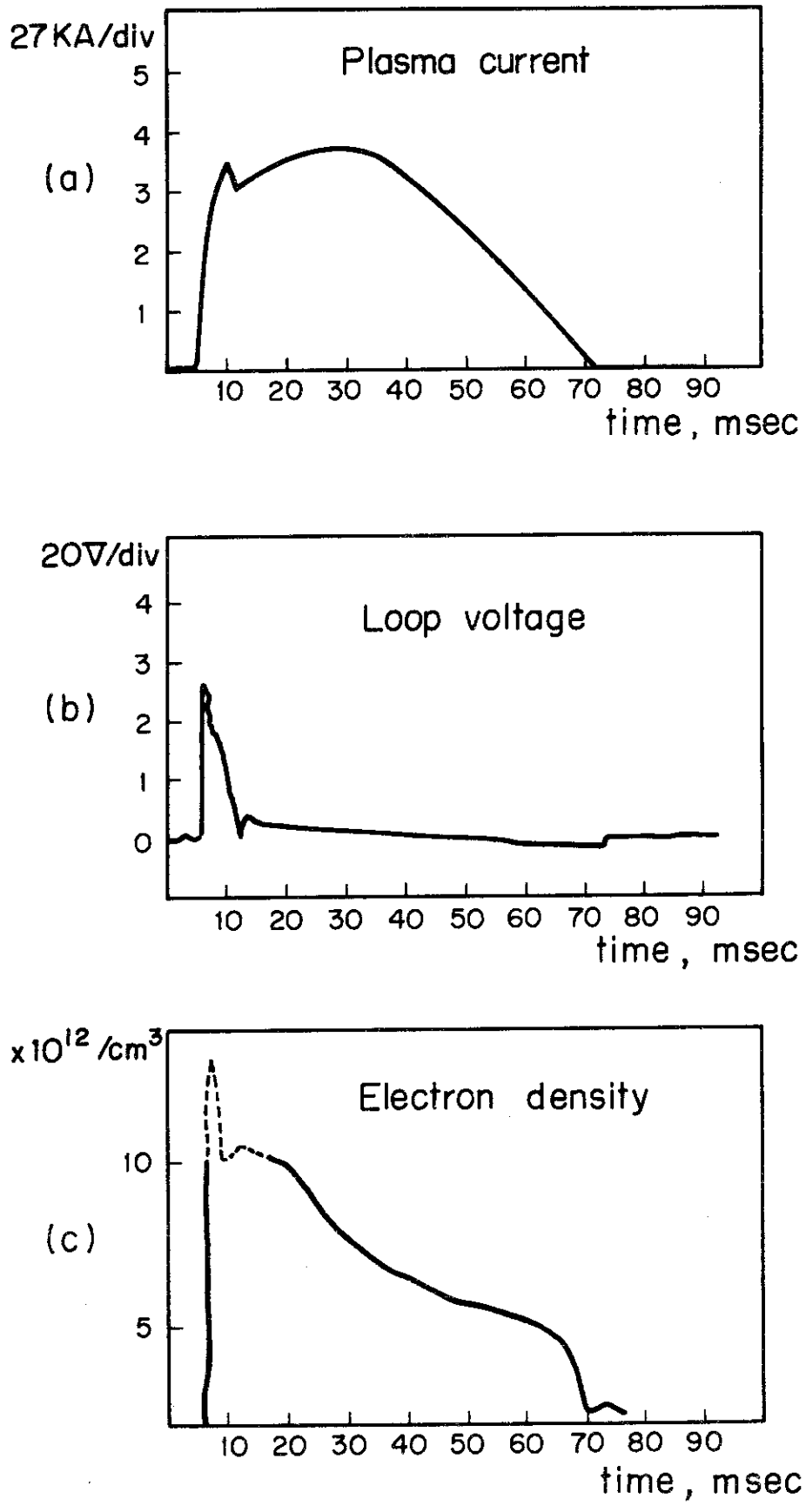

Fig. 17 Time-variations of main plasma parameters for a JFT-2 plasma. (a) plasma current, (b) loop voltage, and (c) average electron density measured with a 4-mm wave interferometer.

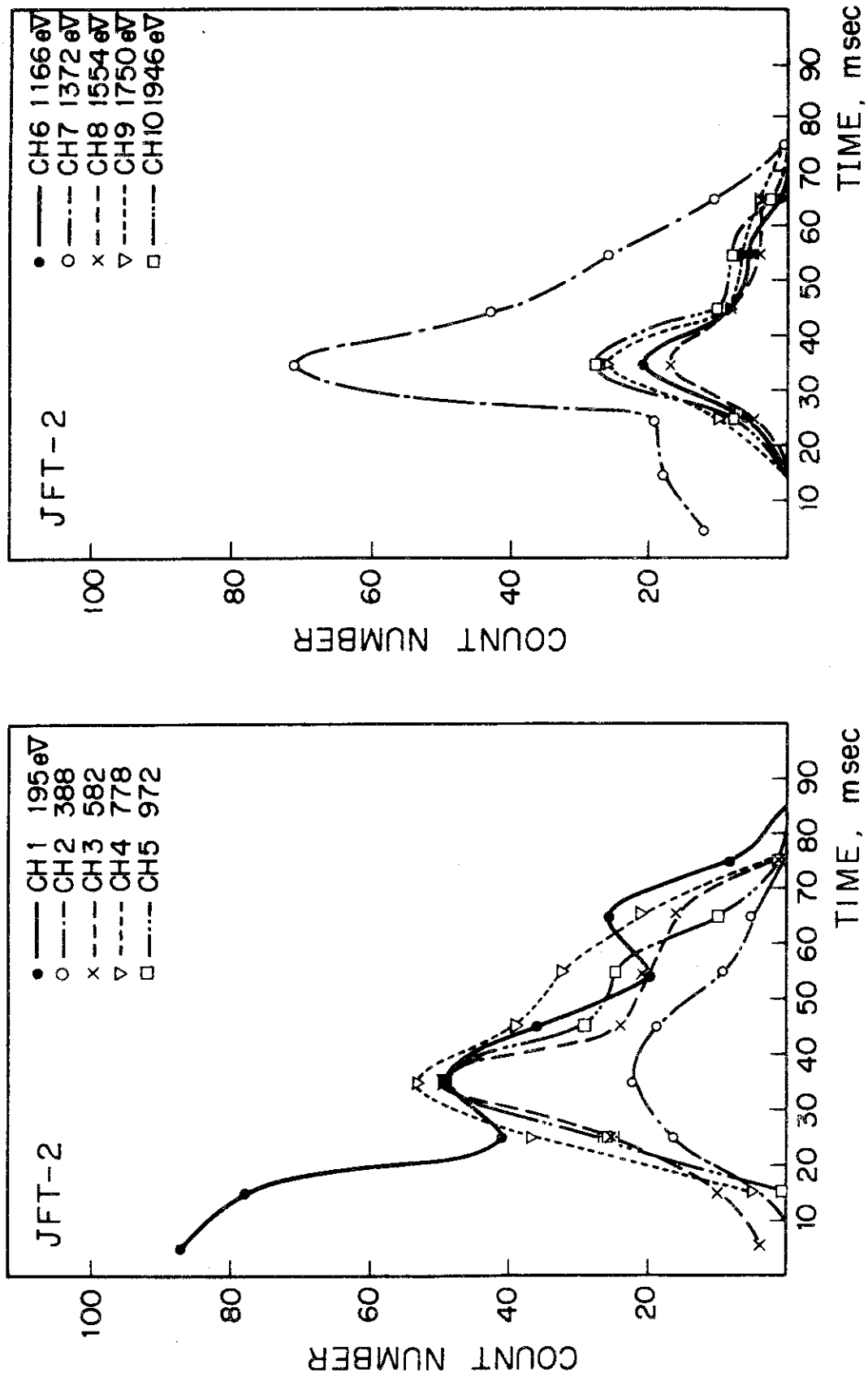

Fig. 18 Time-variations of net particle numbers entering into individual channels for the JFT-2 plasma.

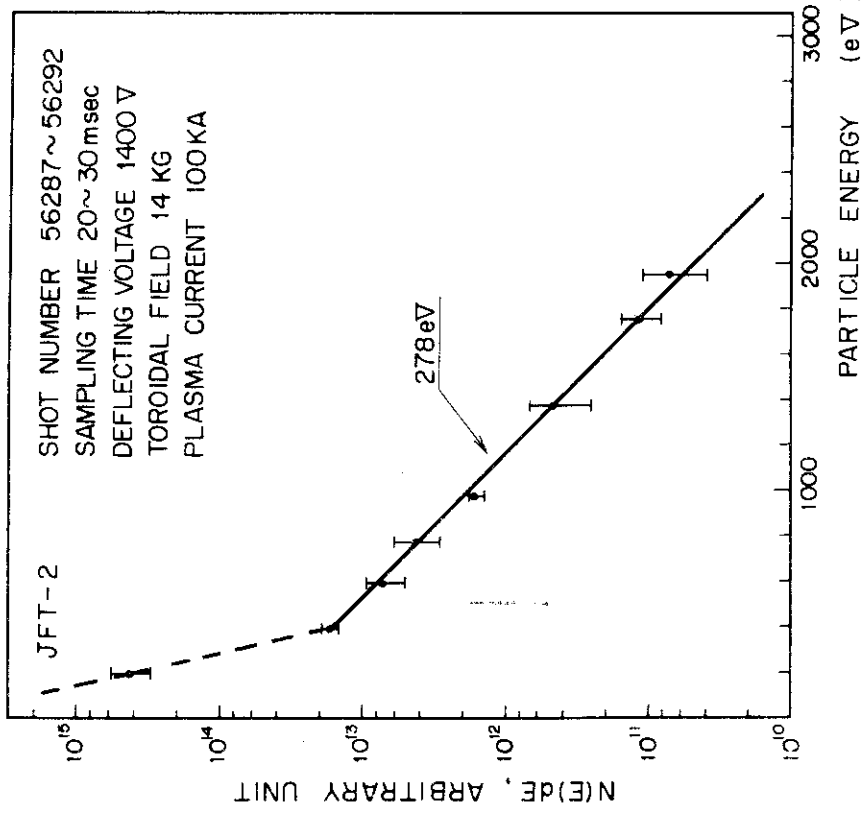

Fig.19(a) Proton energy spectrum observed on the JFT-2 plasma at 20 -- 30 msec.

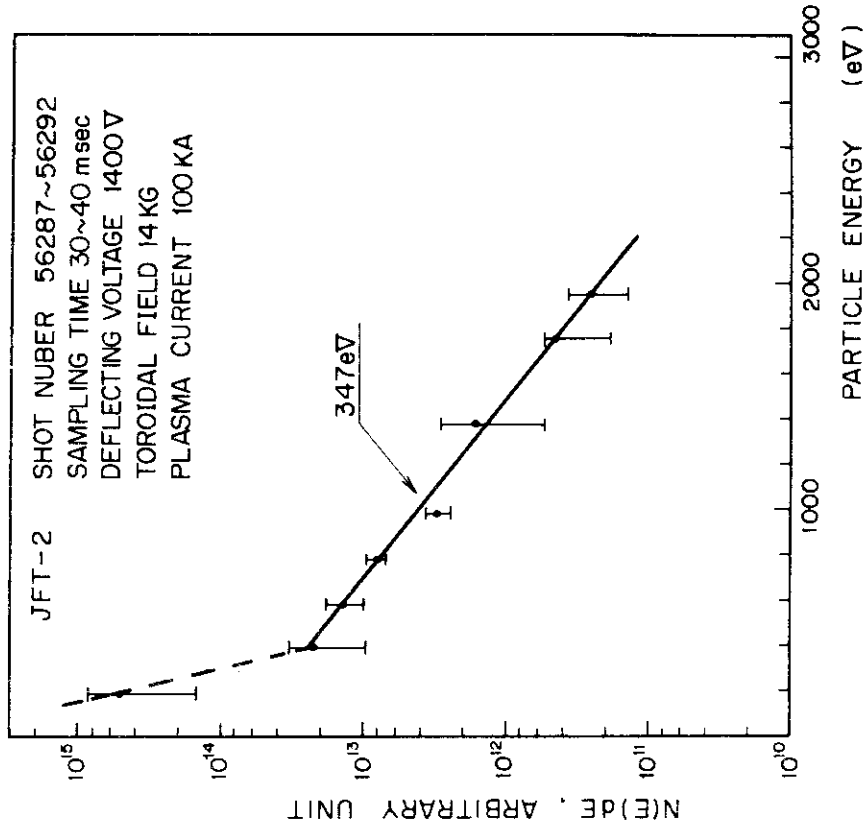

Fig.19(b) Proton energy spectrum observed on the JFT-2 plasma at 30 -- 40 msec.

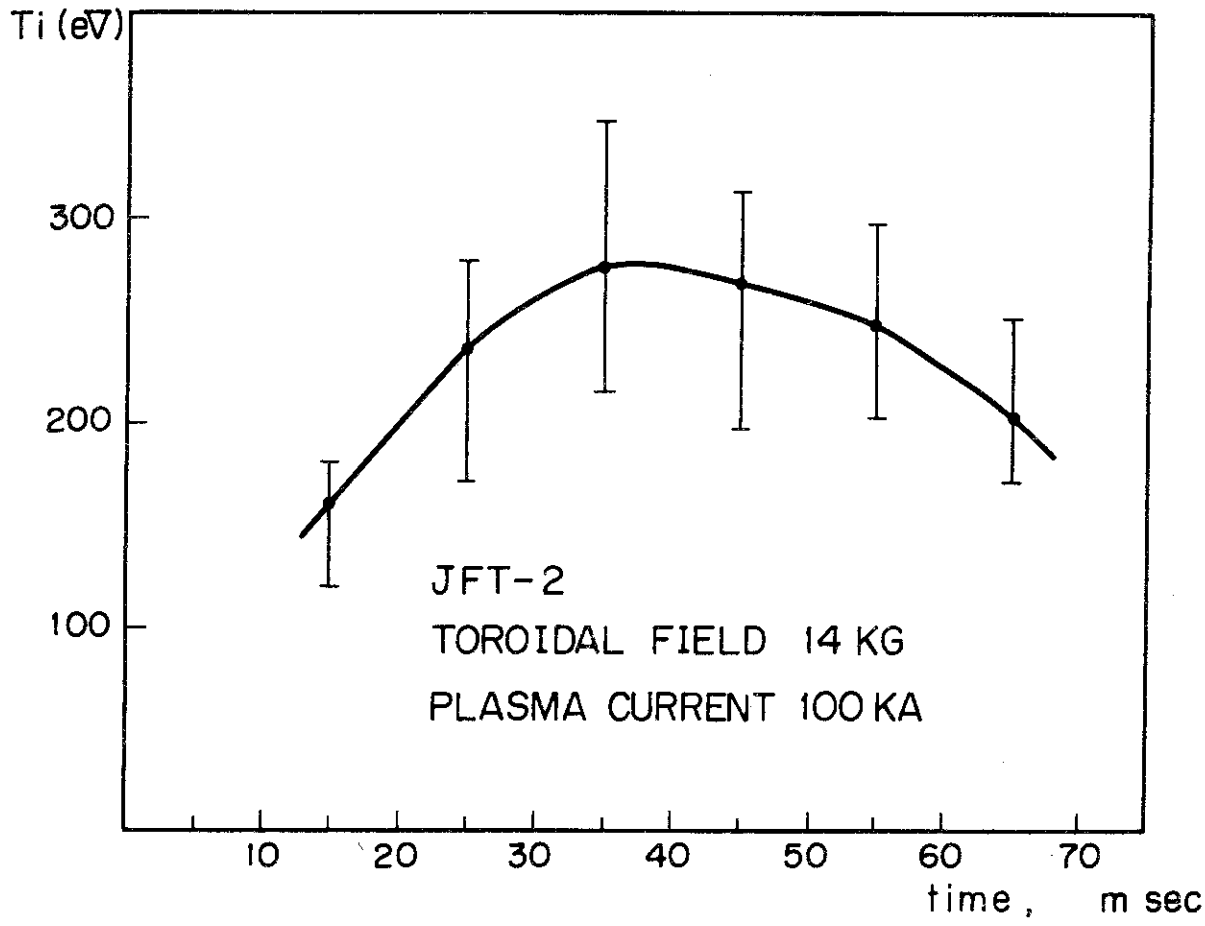

Fig. 20 Time-variation of ion temperature for the JFT-2 plasma.

5. DEPENDENCES OF ION TEMPERATURES ON VARIOUS PARAMETERS

In JFT-2a and JFT-2 devices the dependences of ion temperatures are investigated on various parameters (plasma currents for JFT-2a, and plasma currents, electron densities and toroidal magnetic fields for JFT-2).

First, the results obtained on JFT-2a plasmas are described. In the present experiments hydrogen molecules are injected into a vacuum chamber of JFT-2a by using four fast acting valves for pulsed gas admission.[19c] The hydrogen pressures in plenums of these valves control filling pressures in the vacuum chamber. The plasma currents are varied from 14.3 to 24.6 kAmp. Figure 21(a) shows a typical time-variation of line electron density at a position of major radius R = 63 cm measured with a 4 mm micro-wave interferometer under the condition that the plasma current is 15 kAmp, the toroidal field B_t is 10 kGauss, and the ratio of divertor current to plasma current I_D/I_p is 1.1. In the figure the line density is presented in terms of observed fringe shifts, one fringe shift corresponding to the average electron density of 2.5×10^{12} cm^{-3}. Here we name a peak density at an early time (≃3 msec) as the first peak and at a late time (≃10 msec) as the second peak. The time-variations of ion temperature are measured for a sampling time of 3 msec, as mentioned in section 4. In Fig. 21(b) the peak ion temperatures and the first and second peak-values of average electron density $\bar{n}_e$ are plotted against the plenum pressures of the fast acting valves. In the present measurements the peak ion temperatures are found to be realized nearly at the same time of the second peak density. As seen in Fig. 21(b), the peak ion temperatures and second peak densities are almost independent of the plenum pressures.

The dependence of ion temperatures on plasma currents are shown in Fig. 22(a) and (b), which give the time-variations of ion temperatures for different peak values of plasma currents and the relation between the peak temperatures and peak currents, respectively. The peak values of central electron temperatures are 200 -- 300 eV determined from measurements of ruby laser scattering.[19b,22] The chain line in Fig. 22(b) is obtained from Artsimovich's scaling law[21]

$$T_i = 6 \times 10^{-7} (I_p B_t \bar{n}_e R^2)^{1/3} \qquad (8)$$

where T_i in eV, I_p in amperes, B_t in Gauss, $\bar{n}_e$ in cm^{-3}, and R in cm. This scaling law is deduced from the classical energy transfer from electrons to ions and the neo-classical thermal conduction loss of ions in a plateau

region. The observed dependence of peak ion temperatures on plasma currents may indicate that Artsimovich's scaling law is valid for JFT-2a plasmas within the experimental errors.

Next, we present the results on JFT-2 plasmas. The ranges of parameters are as follows, i.e., plasma currents being from 100 to 170 kAmp, average electron densities from 8 to 18 $\times 10^{12}$ cm^{-3}, and toroidal magnetic fields from 14 to 18 kGauss.

In JFT-2 experiments two kinds of gas supply systems are adopted. One is a continuous gas supply system, which flows hydrogen molecules constantly into a vacuum chamber (continuous admission). Another is a combination of the continuous supply system and an additional pulsed gas supply system with a fast acting valve (continuous and pulsed admissions). The ion temperatures are measured for a sampling time of 10 or 20 msec under various operating conditions, and their time-variations and peak temperatures are determined in a similar way as shown in Fig. 20. Figures 23 to 27 show the dependences of peak ion temperatures on the average central density $\bar{n}_e$, toroidal magnetic field B_t, and plasma current I_p. The data presented in Fig. 23, 24 and 25 are obtained for measurements of continuous and pulsed hydrogen admissions, and in Fig. 26 and 27 for measurements of continuous hydrogen admission. In these experiments the peak values of central electron temperatures from measurements of ruby laser scattering[22] and soft X-ray spectrums[23] are about (2 -- 3) times of peak ion temperatures. It is noted that each dependence is investigated by keeping the other two parameters of three ($\bar{n}_e$, B_t and I_p) constant. The relation between peak temperatures and toroidal magnetic fields has not been examined for the continuous admission experiments.

The solid curves drawn in Figs. 23, 24, 25, 26 and 27 indicate a one-third power function of the quantity in each abscissa. It is found that the peak ion temperatures of JFT-2 plasmas seem to accord with the one-third power dependence of Artsimovich-type law, $T_i \propto (I_p B_t \bar{n}_e)^{1/3}$ within experimental errors.

In Fig. 28 the ion temperatures measured on JFT-2a and JFT-2 plasmas are plotted against $\xi \equiv (I_p B_t \bar{n}_e R^2)^{1/3}$ for the following ranges of parameters;

(i) JFT-2a, $\bar{n}_e = (0.8 -- 1.0) \times 10^{13}$ cm^{-3}, $I_p = (14.3 -- 24.6)$ kAmp, and $B_t = 10$ kGauss,

(ii) JFT-2, $\bar{n}_e = (0.8 -- 1.8) \times 10^{13}$ cm^{-3}, $I_p = (100 -- 170)$ kAmp, and $B_t = (14 -- 18)$ kGauss.

Dark circles and light circles represent JFT-2 experimental data for the measurements of the continuous and pulsed admissions and the continuous admission, respectively. Cross points show the ion temperatures measured on JFT-2a plasmas. It is found that the ion temperatures on JFT-2a and JFT-2 devices vary according to Artsimovich's prediction, $T_i = K\xi = K(I_p B_t \bar{n}_e R^2)^{1/3}$ (K is a numerical constant). The experimental value K_m of the numerical constant K is determined to be

$$K_m = (4.3 -- 6.7) \times 10^{-7} \tag{9}$$

from Fig. 28. The ion temperatures indicated by light circles and cross points are in sufficiently good agreement with Artsimovich's scaling law for $K = 6 \times 10^{-7}$, i.e., Eq. (8).

The straight line A in Fig. 28 is obtained on the assumption that the current distribution and electron density are constant over the minor cross-section. The line B corresponds to the case where the current distribution and electron density have a parabolic profile. The ion temperatures for the continuous and pulse admission experiments on JFT-2 are less than those for the continuous admission experiments by about 20 percents, and also slightly less than the level indicated by the line A. This phenomena is discussed in the following section.

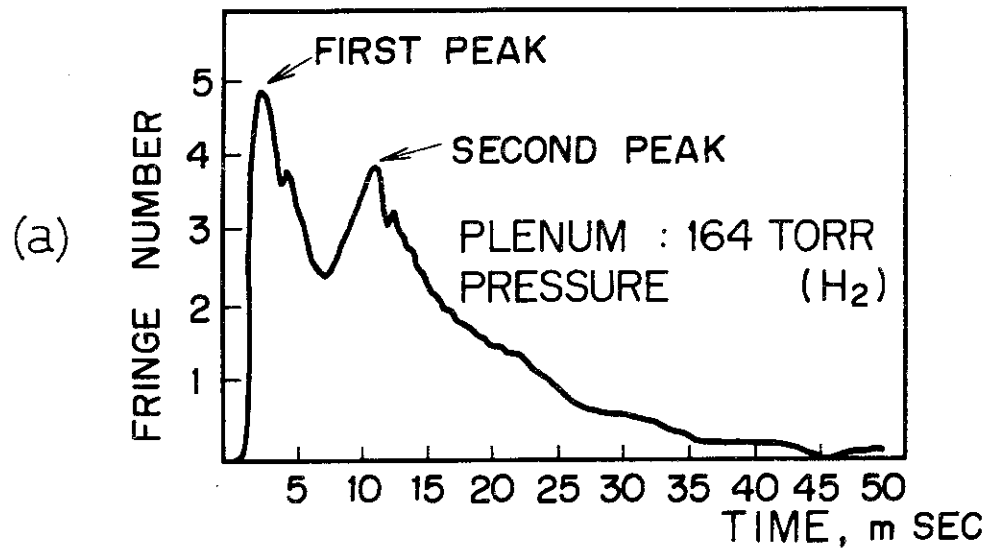

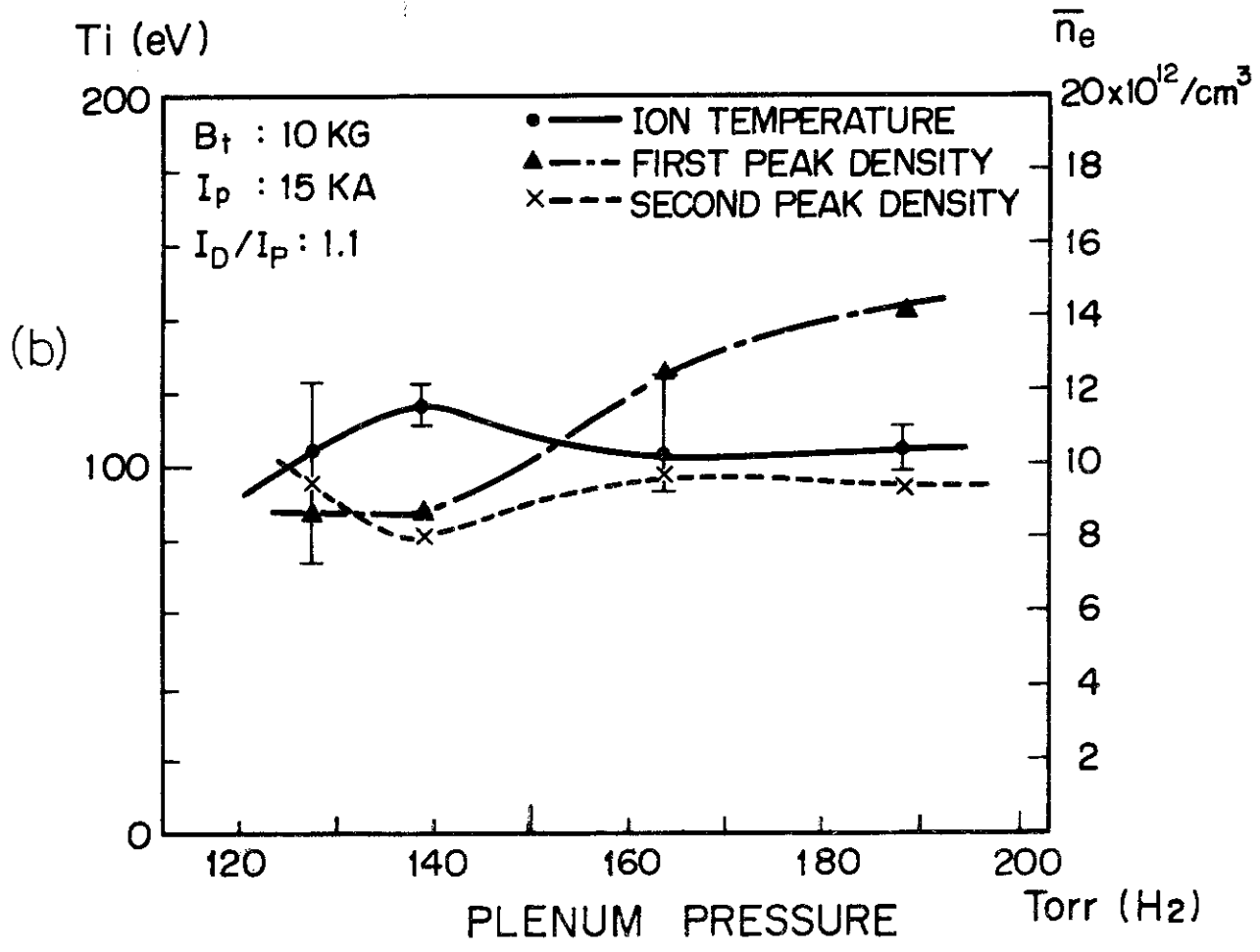

Fig. 21 First and second peaks of electron density (a) and relations among ion temperatures, peak electron densities and plenum pressures of fast acting valves (b) for the JFT-2a plasmas.

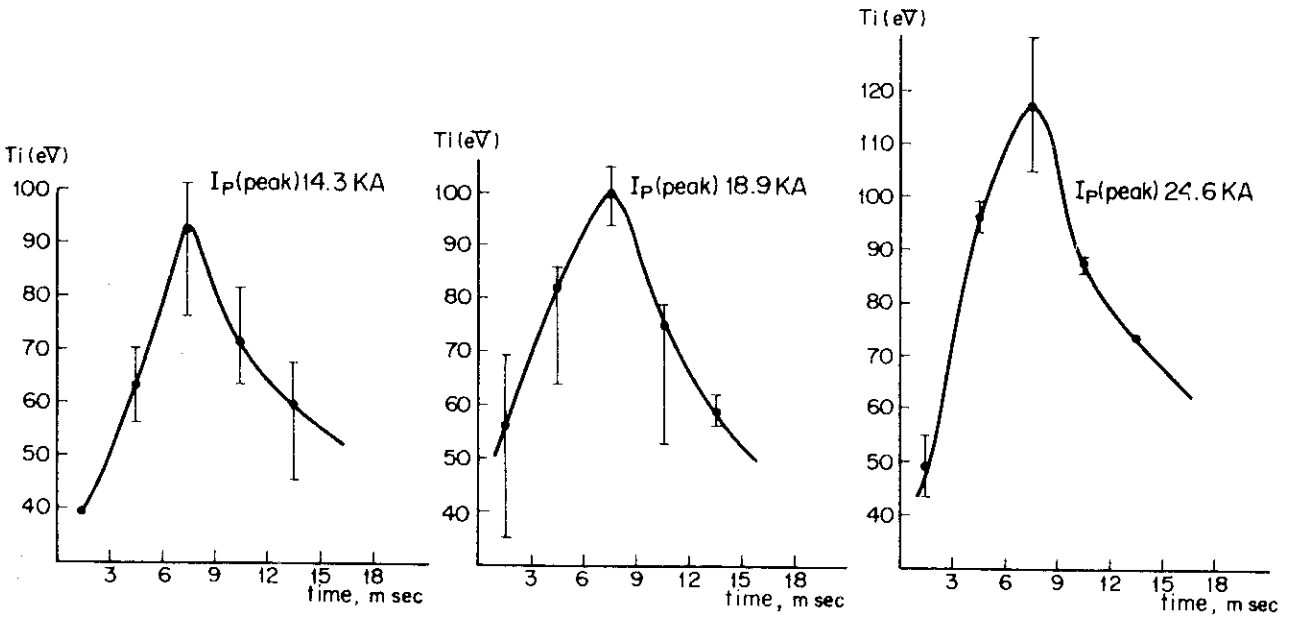

Fig.22(a) Time-variations of ion temperatures of JFT-2a plasmas for different peak currents.

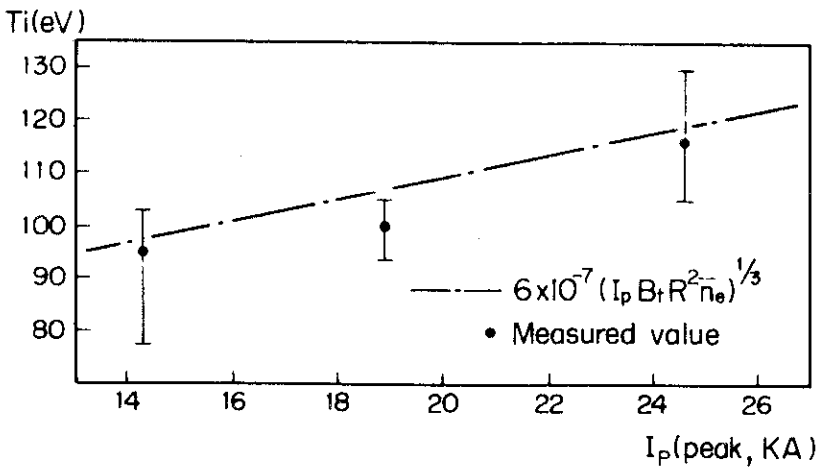

Fig.22(b) Relations between the peak ion temperatures and the peak currents for the JFT-2a plasmas.

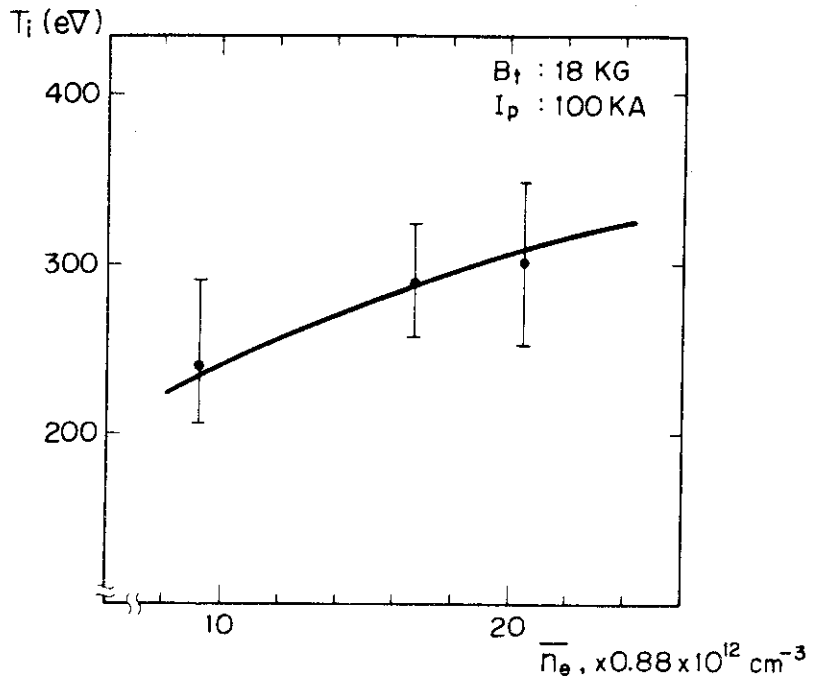

Fig. 23 Dependence of peak ion temperature on the average central electron density (JFT-2, B_t = 18 kGauss, I_p = 100 kAmp, continuous and pulsed hydrogen admissions).

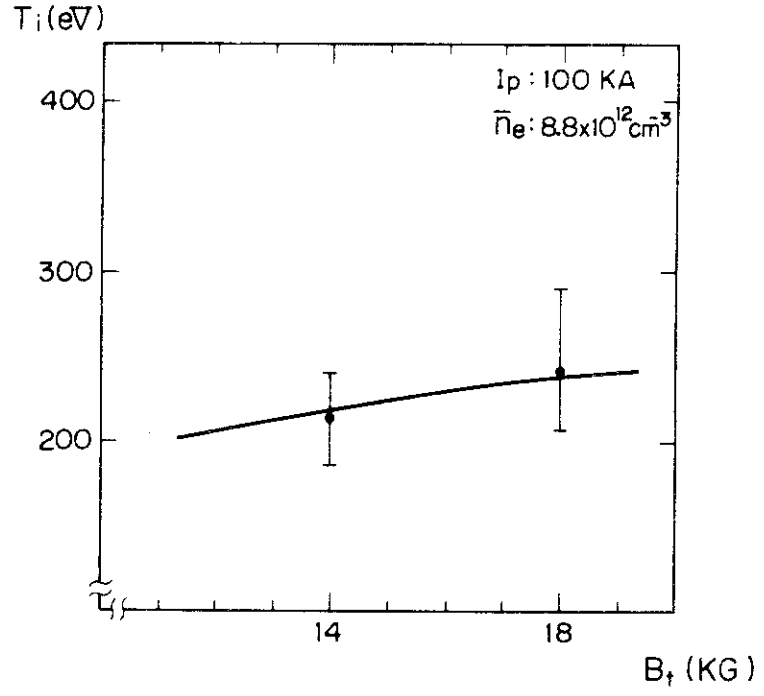

Fig. 24 Dependence of peak ion temperature on the toroidal magnetic field (JFT-2, I_p = 100 kAmp, $\bar{n}_e$ = 8.8 × 10^{12} cm^{-3}, continuous and pulsed hydrogen admissions).

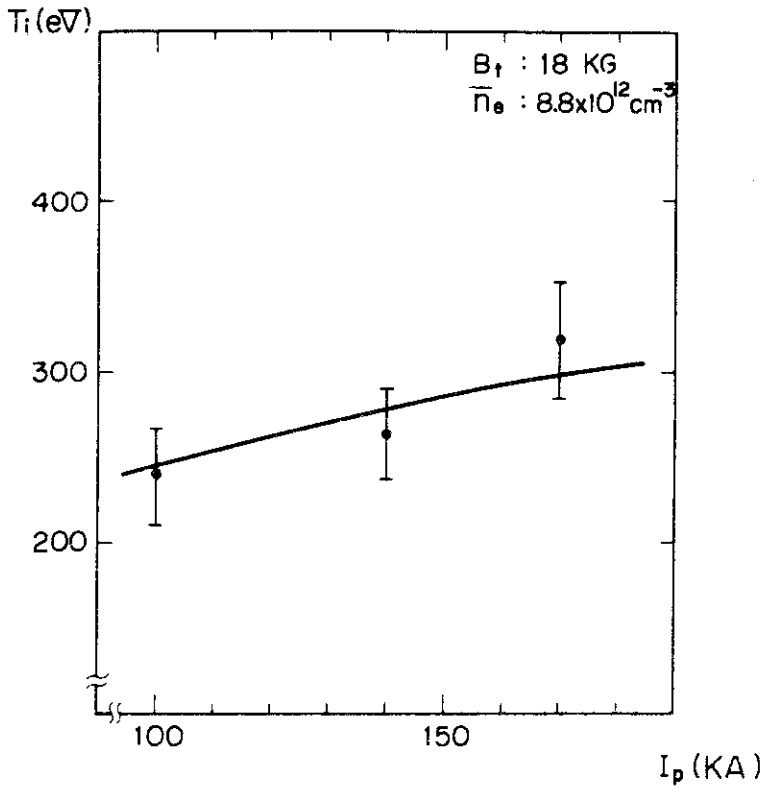

Fig. 25 Dependence of peak ion temperature on the peak plasma current (JFT-2, $\bar{n}_e = 8.8 \times 10^{12}$ cm^{-3}, B_t = 18 kGauss, continuous and pulsed hydrogen admissions).

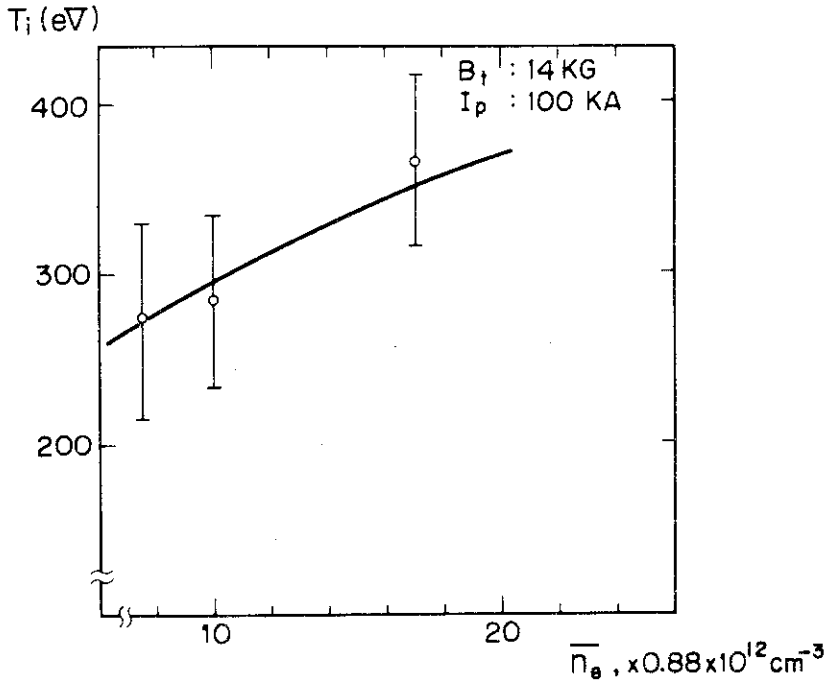

Fig. 26 Dependence of peak ion temperature on the average central electron density (JFT-2, B_t = 14 kGauss, I_p = 100 kAmp, continuous hydrogen admission).

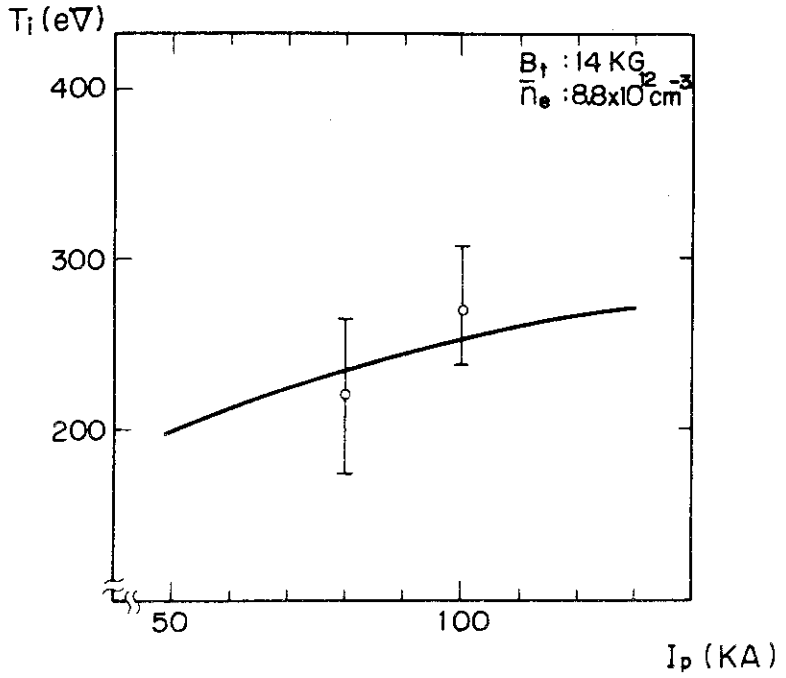

Fig. 27 Dependence of peak ion temperature on the peak plasma current (JFT-2, $\bar{n}_e = 8.8 \times 10^{12}$ cm^{-3}, B_t = 14 kGauss, continuous hydrogen admission).

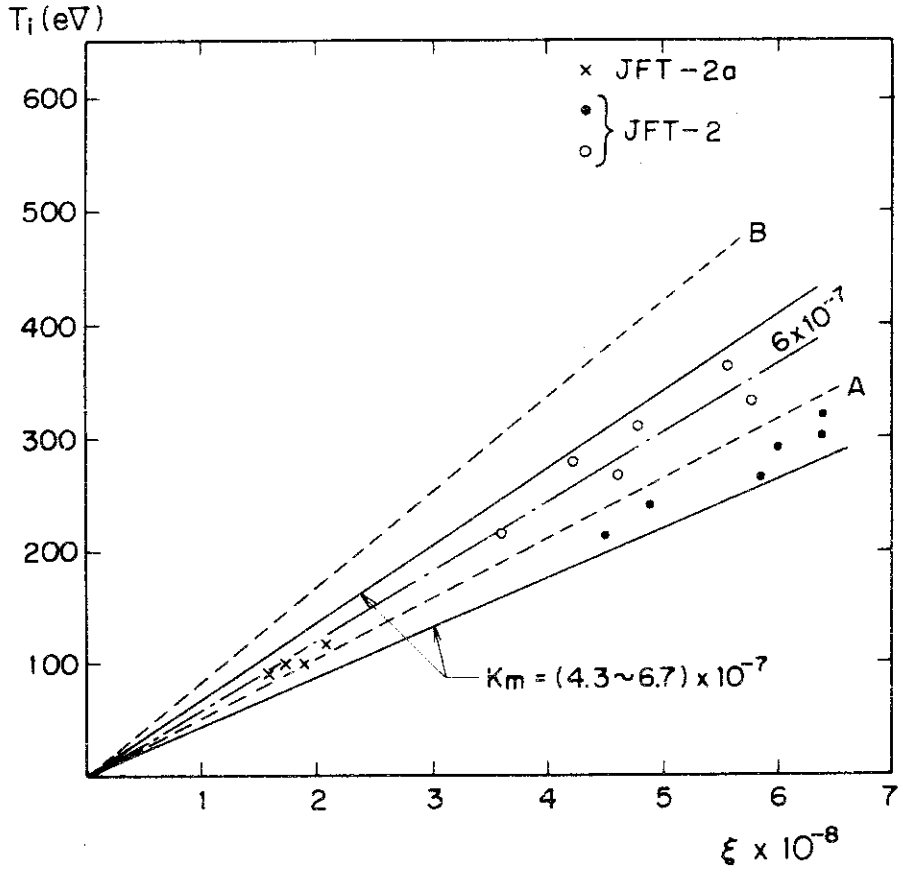

Fig. 28 Relation between the peak ion temperatures and the values of $\xi \equiv (I_p B_t n_e R^2)^{1/3}$.

6. DISCUSSIONS

(i) Conversion effeciency in the charge stripping cell

The ion temperatures measured on JFT-2a plasmas with 10-ch NPEAA are compared to doppler temperatures determined from broadening of Balmer H_α-line emitted from charge-exchanged hydrogen atoms, in order to confirm the validity of the assumption made for the stripping cell efficiency (we adopt the theoretically calculated conversion efficiencies in determining ion temperatures, as described in Section 3). Measurements of H_α-line profiles[24] are simultaneoulsy made with a 1 m Czerny-Turner spectrometer (SPEX 1802) under a typical operating condition of JFT-2a device, i.e., B_t = 10 kGauss, $\bar{n}_e$ (peak) = 1.0×10^{13} cm^{-3}, and I_D/I_p = 1.1. The spectrometer is placed to view the plasma center horizontally in the major-radius direction and to observe the integrated intensity of H_α-line along an optical path. Figure 29 shows comparisons between ion temperatures measured with 10-ch NPEAA and doppler temperatures of H_α-line.(*) In the figure the chain and solid curves are time-variations of doppler temperatures T_D and of ion temperatures T_i, respectively. As seen in the figure $T_i \simeq 2 \times T_D$, and the peak values of T_i and T_D are about 120 eV and 60 eV.

Recently Azumi and Takizuka[25] have given reasonable interpretation of the apparent difference between these two measured temperatures by using numerical simulation calculations on the transportation of neutral hydrogen atoms.(**) According to their calculations, the proton spectrum observed with 10-ch NPEAA are explained to be due to central, hot ions and the measured profiles of line broadening to include additional information about the off-center, warm layer of the plasma column. The measurements of doppler broadenings of H_α-line and the results of the numerical simulation calculations on the transportation of hydrogen atoms seem to support that the assumption made for the conversion efficiency is appropriate.

(*) The observed profile of H_α-line is a combination of broadenings due to higher-temperature, charge-exchanged atoms and lower-temperature (a few eV) atoms corresponding to Franck-Condon neutral atoms from dissociation of hydrogen molecules.[24]

(**) In the numerical calculations, the Boltsmann equation of neutral hydrogen atoms is solved by Monte-Carlo method by considering the charge-exchange and ionization processes.

(ii) Scaling law of ion temperatures

In Fig. 28 the ion temperatures of JAERI-tokamaks have compared with those predicted from the well-known Artsimovich's scaling law.[21,10a,26] This scaling law is derived from the energy balance of ions where the input power from Ohmically heated electrons through classical Coulomb collisions is balanced to the energy loss through ion thermal conductions whose coefficients are given from the neo-classical theory in a plateau region by Galeev and Sagdeev.[27] Although the measured ion temperatures have the parameter dependence predicted from Artsimovich's law $T_i \propto (I_p B_t \bar{n}_e)^{1/3}$ as mentioned in the previous section, there exist sufficient differences between JFT-2 experiments for continuous gas admission and (continuous + additional pulsed) gas admissions.

Under plasma parameters described in the present report, it is confirmed that most of ions are in the plateau region. That is, the equation of $\nu_{1p} < \nu_{pp} < \nu_{2p}$ is held for the JFT-2a plasmas, and $\nu_{1p} \lesssim \nu_{pp} < \nu_{2p}$ for the JFT-2 plasmas, where ν_{pp} is the collision frequency between protons and protons, $\nu_{1p} = (a/R)^{3/2} (v_{Ti}/Rq)$, i.e., the bounce frequency of trapped protons and $\nu_{2p} \simeq v_{Ti}/Rq$. In these equations, a is the minor radius, R the major radius, v_{Ti} the thermal velocity of protons, and q the safety factor.

It is most probable that pulsed hydrogen atoms injected additionally cause the increase the charge-exchange loss, as reported in ORMAK-tokamak experiments.[28] However the induced, charge-exchange loss seems to be much smaller compared with the principle loss, i.e., the thermal conduction loss, because Artsimovich-type dependence is also valid for the additional pulsed admission experiments, as shown in Figs. 23, 24 and 25. The subsidiary charge-exchange loss induced by pulsed injection of molecules may result in lowering of ion temperatures (by a few ten-percents in the present experiments). However the above-mentioned interpretation is only qualitative and is not quantitative. Quantitative measurements of the charge-exchange loss have not yet been performed, since we have not examined the absolute counting efficiencies of the Ceratron multipliers for a proton beam. Thus, the neutral atoms density has not been measured with NPEAA in the present experiments. For Ceratron multipliers used here, only relative counting efficiencies which are necessary to determine ion temperatures have been examined with a proton beam.

We are now calibrating the absolute counting efficiency of Ceratron multiplier by using a proton beam. In the next step, quantitative

measurements of neutral atom density and losses due to the charge-exchange process are to be performed in JAERI-tokamak devices.

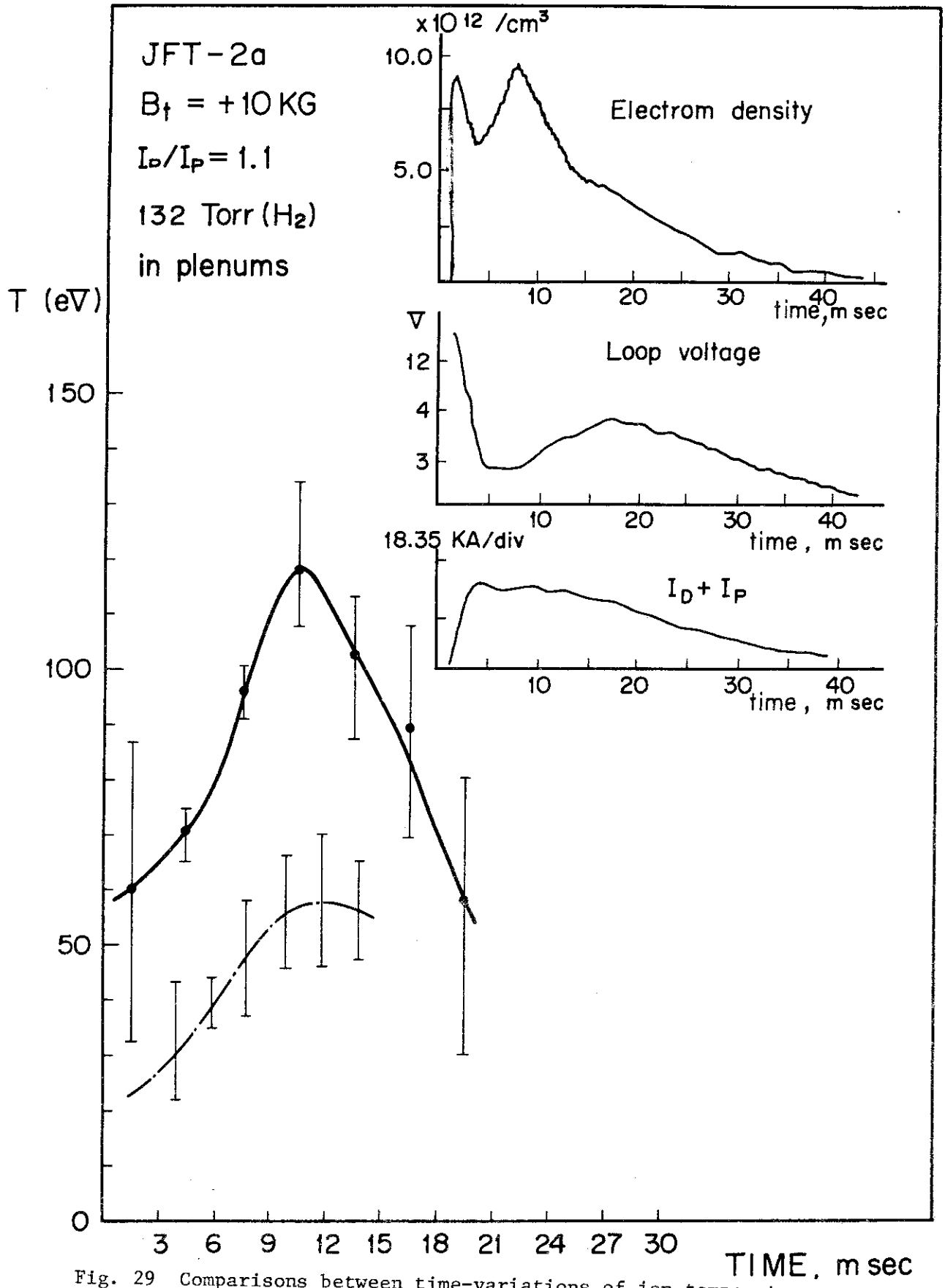

Fig. 29 Comparisons between time-variations of ion temperatures measured from the analysis of charge-exchanged hydrogen atoms and doppler temperatures from broadenings of H_α-line.

7. SUMMARY

In concluding the present report, we summarized our results as follows;

(1) A 10-ch neutral particle energy analyser apparatus has been developed. and constructed to measure hot ion temperatures in JAERI-tokamak devices

(2) The apparatus consists of (a) a 45-degrees parallel plate electrostatic energy analyser equipped with ten Ceratron multipliers as ion detectors, (b) a charge stripping cell of length 20 cm, diameter 40 mm and aperture slits 4 mm in diameter, (c) dry vacuum ion-pumping systems in order to minimize effects of oil-vapor on the detectors and plasmas, and (d) pulse-counting circuits for data acquisition.

(3) Calibration experiments in the analyser apparatus have been performed for determination of ion temperatures.

(4) The 10-ch energy analyser has been energy-calibrated with an electron beam of 100 to 1000 eV. Good agreement between the designed and experimental values is obtained for the particle energy corresponding to each channel and the energy resolution.

(5) The transmission efficiency of particles in the energy analyser has been measured with proton beams of 1, 2 and 3 keV. The transmission efficiency is confirmed to be almsot independent of the incident energy and the channel of the energy analyser.

(6) The conversion efficiency for H_2 gas in the charge stripping cell has been measured for an energy range of 2 to 4 keV. The measured conversion efficiency is in good agreement with the theoretically calculated value in this energy range. The theoretically calculated value is assumed to provide a reasonable conversion efficiency in an energy range higher than 400 eV.

(7) In order to confirm the validity of this assumption on the conversion efficiency, doppler profiles of the Balmer H_α line have been simultaneously measured for the JFT-2a plasmas. It is found the numerical simulation calculations on neutral hydrogen-atoms can explain reasonably the measured results of proton spectrums and H_α - broadening profiles, and that the ion temperatures measured from the present neutral particle analysis can give

the central hot temperatures of the JFT-2a plasmas.

(8) The 10-ch neutral particle energy analyser apparatus has been used to determine ion temperatures of JFT-2a and JFT-2 tokamak plasmas.

(9) The ion temperatures have been measured with a sufficient accuracy from six plasma-shots, i.e., three shots to determine particle signals and three shots to determine back-ground noises. The breadths of relative intensities at individual channels in proton energy spectrums have been estimated by assuming that net particle signals accord with a student-distribution of three samples and 90-percents reliability.

(10) The peak ion temperatures of 80 -- 130 eV and 200 -- 400 eV have been obtained on JFT-2a and JFT-2 devices respectively.

(11) The peak ion temperatures have been about (1/2 -- 1/3) or the central electron temperatures determined from ruby laser scattering or soft X-ray measurements on JFT-2a and JFT-2 plasmas.

(12) The dependences of ion temperatures T_i have been measured on the plasma currents I_p, the toroidal magnetic fields B_t, and the average central electron density $\bar{n}_e$.

(13) The following dependences have been observed for JFT-2a or JFT-2 plasmas;

$$T_i \propto (I_p)^{1/3} \quad \text{for} \quad 15 \leqq I_p \leqq 170 \text{ kAmp},$$
$$T_i \propto (B_t)^{1/3} \quad \text{for} \quad 10 \leqq B_t \leqq 18 \text{ kGauss},$$
and
$$T_i \propto (\bar{n}_e)^{1/3} \quad \text{for} \quad 0.8 \leqq \bar{n}_e \leqq 1.8 \times 10^{13} \text{ cm}^{-3}.$$

(14) The measured dependence of ion temperatures on various parameters have been compared and is in good agreement with the scaling law by Artsimovich $T_i = K_m \cdot (I_p B_t \bar{n}_e R^2)^{1/3}$ with the numerical constant $K_m = (4.3 \text{ -- } 6.7) \times 10^{-7}$.

(15) The results obtained in the present report, in particular, the facts above-mentioned in (11) and (14) of this section indicate that ion temperature of JFT-2a and JFT-2 plasma are very similar to ones observed in other tokamak devices.

ACKNOWLEDGEMENTS

The authors are grateful to Drs. N. Fujisawa, Y. Shomomura and other members of JFT-2, -2a and diagnostic groups for their co-operation and discussions, and to Mr. S. Kunieda and his groups for their operation of plasma devices.

We also appreciate many fruitful suggestions by Drs. M. Azumi and T. Takizuka through their numerical calculations. We would like to express our gratitude to Drs. M. Tanaka and S. Mori for their continuous encouragement to the present work.

REFERENCES

1) V. V. Afrosimov, I. P. Gladkovskii, Yu. S. Gordeev, I. F. Kalinkevich, M. P. Petrov and N. V. Fedorenko : Soviet Phys. - Tech. Phys. 5 (1961) 1389.

2) V. V. Afrosimov, I. P. Gladkosvkii, A. I. Kislyakov and M. P. Petrov : Soviet Phys. - Tech. Phys. 8 (1963) 147.

3) V. V. Afrosimov and M. P. Petrov : Soviet Phys. - Tech. Phys. 12 (1968) 169.

4) D. S. Prono and C. B. Wharton : Plasma Phys 15 (1973) 253.

5) N. Noda, K. Sato, R. Akiyama, N. Inoue and T. Uchida : Nucl. Fusion 12 (1972) 607.

6) H. H. Fleischmann and R. G. Tuckfield, Jr. : Nucl. Fusion 8 (1968) 81.

7) C. F. Barnett and J. A. Ray : Nucl. Fusion 12 (1972) 65.

8) J. D. Ferguson and D. E. Kidd : in Controlled Fusion and Plasma Physics, Proc. 5th European Conf. Grenoble, (1972) vol.1 57.

9) V. V. Afrosimov, I. P. Gladkovskii, Yu. S. Gordeev, I. F. Kalinkevich, M. P. Petrov and N. V. Fedorenko : Soviet Phys. - Tech. Phys. 5 (1961) 1378.

10a) TFR Group : EUR-CEA-FC 778 (July 1975).

10b) B. Coppi et al. : Report of Massachusetts Institute of Technology, Research Laboratory of Electronics PRR-7524 (October, 1975), E. Apgar and D. Pappas : private communication.

11a) V. V. Afrosimov, E. L. Berezovskii, I. P. Gladkovskii, A. I. Kislayakov, M. P. Petrov and K. A. Sadovnikov : Soviet Phys. - Tech. Phys. 20 (1975) 33.

11b) C. F. Barnett et al. : ORNL - 4896 (1972).

11c) P. E. Stott : Plasma Phys. 18 (1976) 251.

12) S. Yano, H. Shirakata, K. Takahashi, A. Kitamura and T. Makino : JAERI-M 5276 (May 1973) in Japanese.

13) A. Kitamura, K. Takahashi and S. Yano : JAERI-M 5275 (May 1973) in Japanese.

14) G. A. Harrower : Rev. Sci. Inst. 26 (1955) 850.

15) N. Noda : J. Phys. Soc. Japan 41 No.2.

16) D. W. Koopman : Phys. Rev. 154 (1967) 79.

17) D. W. Koopman : Phys. Rev. 166 (1968) 57.

18) S. K. Allison : Rev. Mod. Phys. 30 (1958) 1137.

19a) M. Yoshikawa et al. : in Plasma Physics and Controlled Nuclear Fusion Research, Proc. 5th. International Conf. Tokyo, IAEA (Vienna, 1974)

vol. 1, 17.

19b) Y. Shimomura et al. : Private Communication (to be published in Physics of Fluids).

19c) Y. Shimomura et al. : JAERI-M 6102 (April 1975).

20) N. Fujisawa et al. : in Plasma Physics and Controlled Nuclear Fusion Research, Proc. 5th, International Conf. Tokyo, IAEA (Vienna, 1974) vol. 1, 3.

21) L. A. Artsimovich : Nucl. Fusion 12 (1972) 215.

22) T. Matoba : private communication.

23) JFT-2 group : private communication.

24) S. Kasai et al.: to be published.

25) M. Azumi and T. Takizuka : to be published.

26) E. P. Gorbunov, V. S. Zaverjaev and M. P. Petrov : in Controlled Fusion and Plasma Physics, Proc. 6th, European Conf. Moscow, vol. 1, 1.

27) A. A. Galeev and R. Z. Sagdeev : Soviet Phys. - JETP 26 (1968) 233.

28) L. A. Berry, J. F. Clarke and J. T. Hogan : Phys. Rev. Letters 32 (1974) 362,
J. F. Clarke : ORNL-TM-4585 (May 1974).